PNL-5240
UC-70

2F

An In Situ Vitrification Pilot-Scale Radioactive Test

C. L. Timmerman
K. H. Oma

October 1984

Prepared for the U.S. Department of Energy
under Contract DE-AC06-76RLO 1830

Pacific Northwest Laboratory
Operated for the U.S. Department of Energy
by Battelle Memorial Institute

Battelle

PNL-5240

DISCLAIMER

PACIFIC NORTHWEST LABORATORY
operated by
BATTELLE
for the
UNITED STATES DEPARTMENT OF ENERGY
under Contract DE-AC06-76RLO 1830

Printed in the United States of America
Available from
National Technical Information Service
United States Department of Commerce
5285 Port Royal Road
Springfield, Virginia 22161

NTIS Price Codes
Microfiche A01

Printed Copy

Pages	Price Codes
001-025	A02
026-050	A03
051-075	A04
076-100	A05
101-125	A06
126-150	A07
151-175	A08
176-200	A09
201-225	A010
226-250	A011
251-275	A012
276-300	A013

PNL-5240
UC-70

AN IN SITU VITRIFICATION PILOT-SCALE RADIOACTIVE TEST

C. L. Timmerman
K. H. Oma

October 1984

Prepared for
the U.S. Department of Energy
under Contract DE-AC06-76RLO 1830

Pacific Northwest Laboratory
Richland, Washington 99352

ACKNOWLEDGMENTS

Several fellow researchers and technicians contributed to and made this test a success. Listed below are these contributors and their areas of assistance:

W. F. Bonner - Program Guidance
J. L. Buelt - System Design & Test Operation
J. G. Carter - System Design & Test Operation
R. K. Farnsworth - Test Operation
V. F. FitzPatrick - Program Management & Test Operation
S. D. Harris - Test Operation
C. R. Hymas - Test Operation
J. M. Latkovich - Program Guidance
M. L. Longaker - Test Operation & Analysis
J. H. Reeves - Radionuclide Gamma Analysis
C. W. Thomas - Radionuclide Alpha and Beta Analysis

SUMMARY

Pacific Northwest Laboratory (PNL) is developing in situ vitrification (ISV) as an in-place stabilization technique for selected liquid radioactive waste disposal sites. The process melts the wastes and surrounding soil to produce a durable glass and crystalline waste form. These ISV process development testing and evaluation studies are being conducted for the U.S. Department of Energy. This report discusses the results of an ISV pilot-scale test conducted in June of 1983 in which soils contaminated with actual radioactive transuranic and mixed fission product elements were vitrified.

The primary objectives of the radioactive test were to 1) demonstrate containment and confinement of the radioactive material, 2) verify equipment performance of the power and off-gas systems, 3) identify losses to the off-gas system, and 4) characterize the behavior of the radioactive material in the vitrified soil.

The test successfully demonstrated the processing containment of radionuclides both within the vitrified mass and in the off-gas system. No environmental release of radioactive material was measured during testing operations. The vitrified soil had a greater than 99% retention of all radionuclides. Losses to the off-gas system varied from $\leq$0.03% for particulate materials (plutonium and strontium) to 0.8% for cesium which is a more volatile element. The off-gas system effectively contained both volatile and entrained radioactive materials. Analysis of the vitrified soil revealed that all radionuclides were distributed throughout the vitrified zone, some more uniformly than others. No migration of radionuclides outside the vitrification zone occurred, as indicated by analysis of soil samples from around the block. Previous waste form leaching studies (Oma et al. 1983 and Timmerman et al. 1983) indicate an acceptable durability of the ISV product.

CONTENTS

FIGURES

FIGURES (Contd)

TABLES

INTRODUCTION

The in situ vitrification (ISV) concept (Brouns et al. 1983) for converting contaminated soil to an inert crystalline and glass form was first tested in August 1980. In the ISV process, electrical current is passed among an array of four electrodes inserted in the ground around the waste to be stabilized. Joule heating from the process melts the soil, thus encapsulating the radioactive contaminants. This program has been sponsored by the U.S. Department of Energy's (DOE's) Richland Operations Office for potential application to Hanford sites.

A major objective of the program during FY 1983 was to vitrify actual radioactive materials in place. To accomplish this, a modular pilot-scale off-gas treatment unit for the radioactive field test was constructed and installed in a mobile semi-trailer. The power system and off-gas treatment system were improved designs, building upon experience gained with the initial pilot-scale field test system. Two nonradioactive tests were performed with the mobile pilot scale system to provide equipment checkout and operator training prior to the radioactive field test. These tests are referred to as pilot-scale cold tests (PSCTs 1 and 2). A successful pilot-scale radioactive test (PSRT) was performed in June 1983, using a make-up site in which known quantities of ^{241}Am, ^{239}Pu, ^{238}Pu, ^{137}Cs, ^{106}Ru, ^{90}Sr, and ^{60}Co were placed. The initial 19 L waste package of soil contained 600 nCi/g transuranic (TRU) waste and 30,000 nCi/g mixed fission products.

This report presents the performance test results of the radioactive test and a system and test description. Data from the nonradioactive operational acceptance tests are also included for comparison. Table 1 summarizes the objectives and results of the three pilot-scale field tests.

TABLE 1. Summary of Results of Pilot-Scale Cold and Radioactive Tests (mobile system)

Test	Objectives	Results
PSCT 1	Vitrify simulated waste package Perform operator training and equipment checkout	Successful vitrification of waste package. Off-gas system maintained total containment of volatile elements. Identification of items requiring upgrade.
PSCT 2	Vitrify simulated waste package Verify correct operation of system upgrade	Successful vitrification of waste package and successful test of system upgrade.
PSRT	Vitrify a makeup site containing known quantities of radionuclides	Successful vitrification with no release of radioactivity.

PROCESS DESCRIPTION

During ISV, contaminated soils are stabilized by inserting electrodes in the soil and establishing an electric current between the electrodes. Figure 1 illustrates the process sequence. For startup, a small amount of specially prepared graphite is placed in paths between the electrodes on the soil surface. Dissipation of power through the starter material creates temperatures high enough to melt a layer of soil, thereby establishing a molten, conductive path. This molten zone continues to grow in size, provided sufficient power is supplied to overcome heat losses. At the high temperatures (>1700°C) created, organic materials pyrolyze; the remaining ash, along with other noncombustible waste materials, dissolves or becomes encapsulated in the molten soil. Natural convective currents in the molten soil help distribute the waste materials uniformly. Upon cooling, a durable glass and crystalline waste form is created. Off gas from the process is collected and treated. If ground subsidence occurs during ISV, uncontaminated soil can be backfilled over the site.

The process operation is based on extensive joule-heated melter work performed at PNL for various nuclear waste immobilization projects (Buelt et al. 1979). The joule-heating principle operates by internal resistance heating of

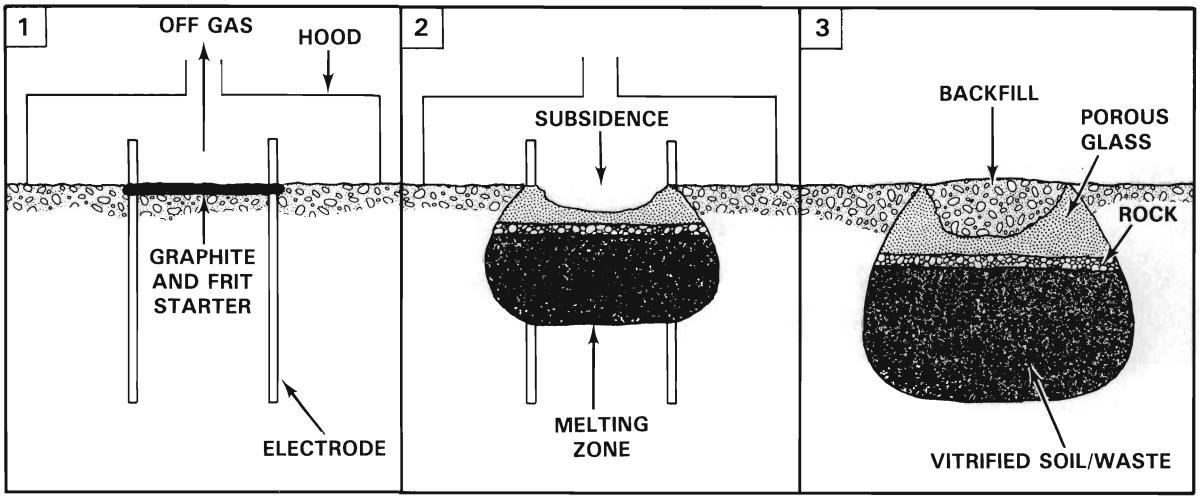

FIGURE 1. In Situ Vitrification Process Sequence

the conducting material as an electric current passes through the molten media. In ISV, the resistance decreases as the molten mass grows; therefore, to maintain a power level high enough (according to the formula $P = I^2R$) to continue melting more soil, the current must be increased. To accomplish this, the amperage is increased by using a power transformer with multiple voltage taps.

At startup, the ISV process requires a high voltage potential and low amperage. As the melt progresses and resistance decreases, the lower voltage taps on the power transformer allow increased amperage to the melt, thus maintaining a high power level into the melt. The process will continue until heat losses from the melt approach the energy delivered to the molten soil via the electrodes.

A hood over the vitrification zone is maintained under a slight vacuum to contain any hazardous gases or particulates that may be released. This hood also provides support for the electrodes. The vacuum on the hood is supplied by the off-gas treatment system, which scrubs and filters any hazardous components from the off-gas stream.

PILOT-SCALE RADIOACTIVE TEST SYSTEM

The pilot-scale radioactive test system utilizes four electrodes with a 1.2 m separation and consists of a power control unit, an off-gas containment hood over the waste site, and an off-gas treatment system housed in a portable semi-trailer (see Figure 2). Prior to the radioactive test, this same system was used on two nonradioactive tests: pilot-scale cold tests 1 and 2.

POWER SYSTEM DESIGN

The pilot-scale power system utilizes a Scott-Tee connection to transform a three-phase input to a two-phase secondary load on diagonally opposed electrodes in a square pattern. The 500 kW power supply may be either voltage or current regulated. The alternating current primary is rated at 480 V, 600 A, 3 phase, and 60 Hz. The 3 phase input feeds a Scott-Tee connected transformer (see Figure 3) providing a 2 phase secondary. The transformer has four separate voltage tap settings--1000 V, 650 V, 430 V, and 250 V. Each voltage tap has a corresponding amperage rating of 250 A, 385 A, 580 A, and 1000 A per

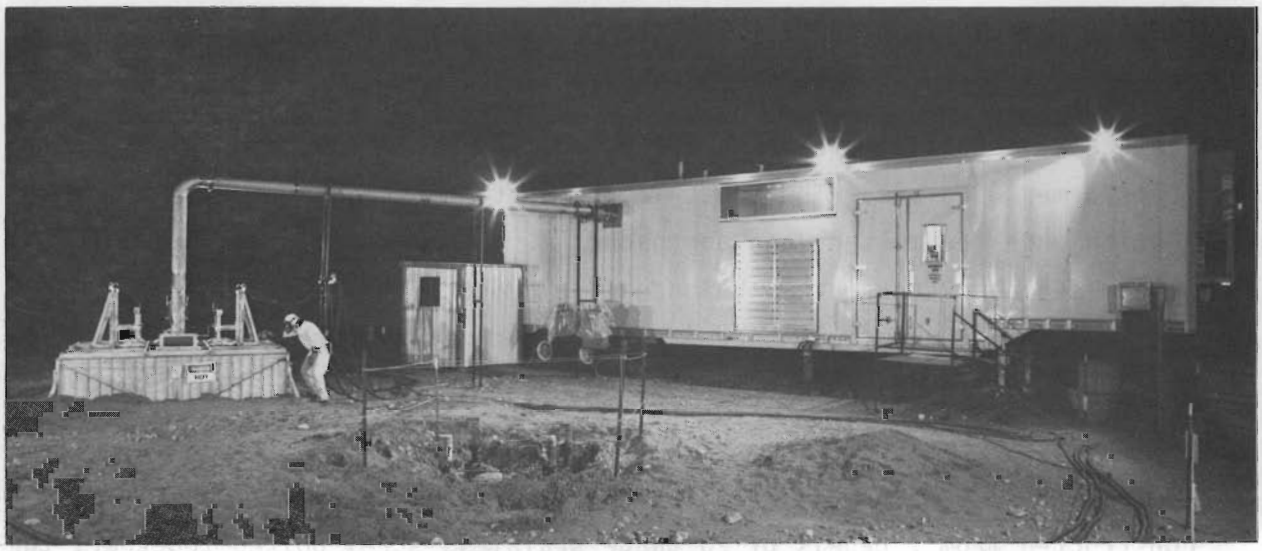

FIGURE 2. Pilot-Scale ISV Hood and Process Trailer

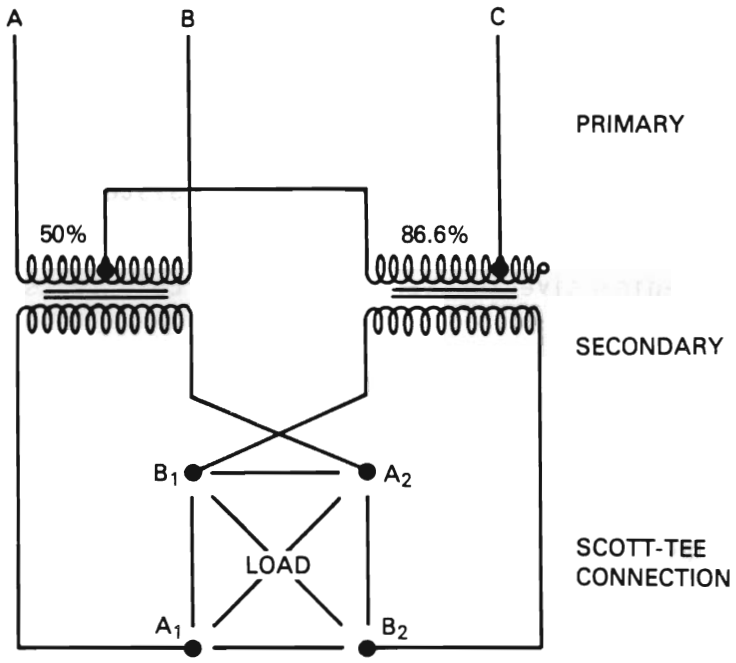

FIGURE 3. Scott-Tee Electrical Connection for the Pilot-Scale System

phase, respectively. The amount of 3 phase input power delivered to the transformer is controlled by adjusting the conduction angle of the thyristor switches located in each of the three input lines. These switches, in conjunction with selectable taps on the transformer secondary, regulate the amount of output power deliverable to both secondary phases.

The Scott-Tee setup requires transformer taps at 50 and 86.6% of the primary transformer windings. The Scott-Tee connection provides an even power distribution when the molten zone approaches a uniform resistance load. The primary and secondary current is balanced for a Scott-Tee system when a balanced load exists. During all three tests this power system proved very effective in maintaining a balanced load to the electrodes.

OFF-GAS CONTAINMENT AND ELECTRODE SUPPORT HOOD

Constructed from 7 panels of 20 gauge stainless steel bolted together, the off-gas containment and electrode support hood (see Figure 4) is 3.05 m (10 ft)

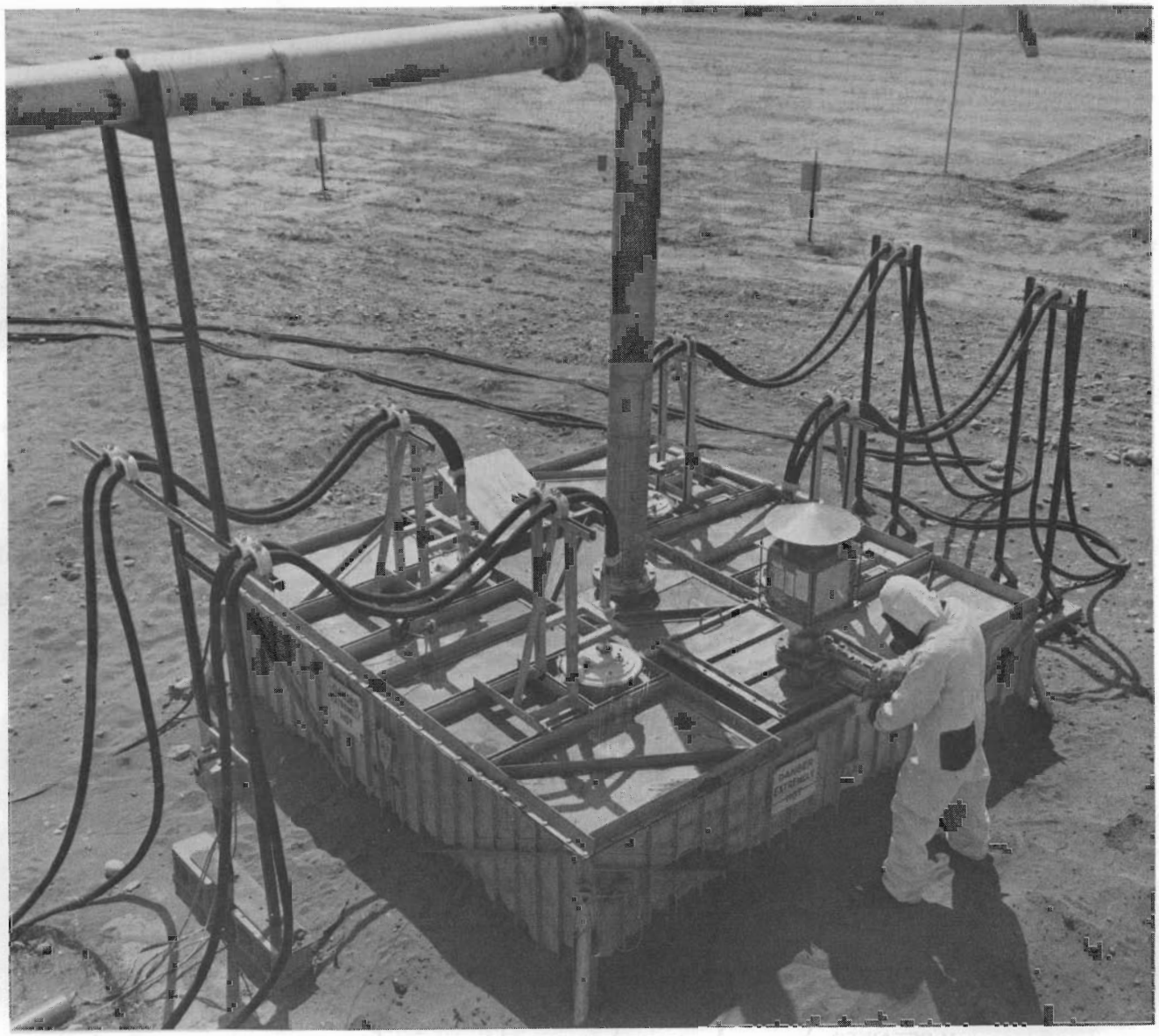

FIGURE 4. Off-Gas Containment and Electrode Support Hood

square by 0.9 m (3 ft) high. Four leveling supports attached to the side panel corners can also be unbolted. The hood is designed to withstand an 18 cm (7 in.) water vacuum.

The off-gas containment and electrode support hood includes a viewing port and an access port. Built into the access port is a valve and High Efficiency Particulate Air (HEPA) filter assembly for regulating the vacuum on the hood. A center off-gas port allows direct coupling of the hood to the processing van

and off-gas treatment system. The hood is equipped with a heat shield installed under the center top panel to protect the hood from heat radiating from the partially molten surface during processing.

The hood is sealed to the surface of the soil surrounding the zone to be vitrified by a flexible skirt of tightly woven, high-temperature resistant fiber attached to the bottom of all side panels. This skirting extends ~0.6 m (2 ft) away from the hood, allowing for a hood-to-ground seal when covered with a layer of soil.

Electrical bus bars, connected to the graphite electrodes, protrude through the hood and are surrounded by electrically insulated sleeves which allow adjustment of the electrode position (Figure 5). The electrodes and bus bars are supported by insulators above the sleeve. The insulators are designed to withstand movement of the molten mass against the electrodes from convective currents and the gravitational and buoyant forces exerted on the electrodes.

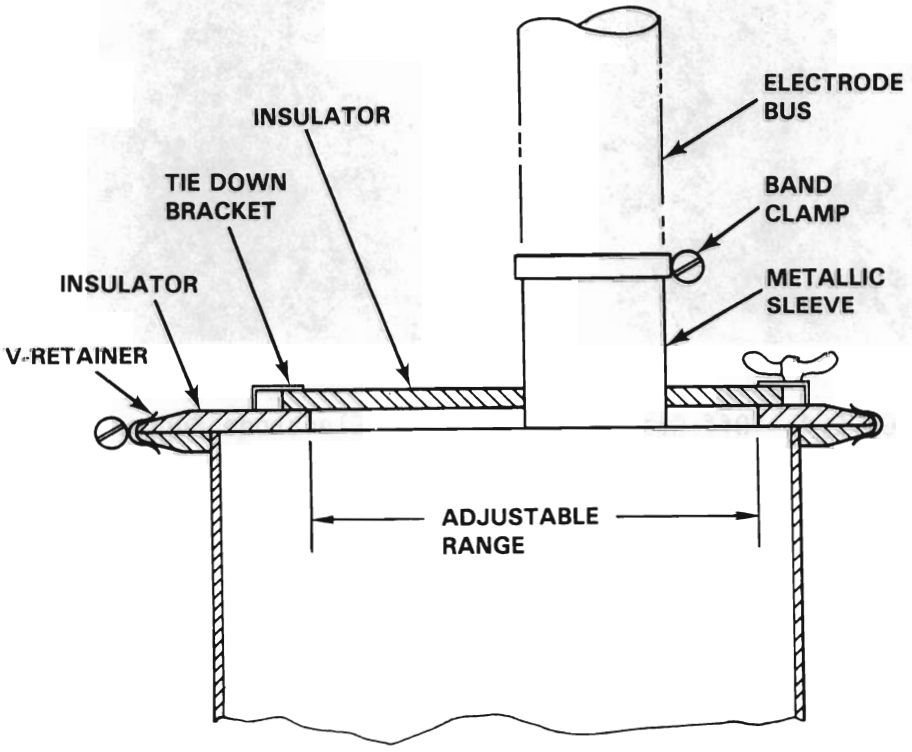

FIGURE 5. Design of Hood Feed-Through for Electrode Bus Bar

OFF-GAS TREATMENT SYSTEM

The off-gas system is shown schematically in Figure 6. The off gas passes through a venturi-ejector scrubber and separator, Hydro-Sonic® scrubber, separator, condenser, another separator, heater, two stages of HEPA filtration, and a blower. Liquid to the two wet scrubbers is supplied by two independent scrub recirculation tanks, each equipped with a pump and heat exchanger. The entire off-gas system has been installed in a 13.7 m (45 ft) long semi-trailer to facilitate transport to a waste site. Equipment layout within the van is illustrated in Figure 7. All off-gas components except the second stage HEPA filter and blower are housed within a removable containment module pictured in Figure 8, which has gloved access for remote operations and is maintained under a slight vacuum.

Heat is removed from the off gas by a closed loop cooling system, which consists of an air/liquid heat exchanger, a coolant storage tank, and a pump. A 50% water/ethylene glycol mix is pumped from the storage tank through the shell side of the condenser and the two scrub solution heat exchangers, then through the air/liquid exchanger, where heat is removed from the coolant.

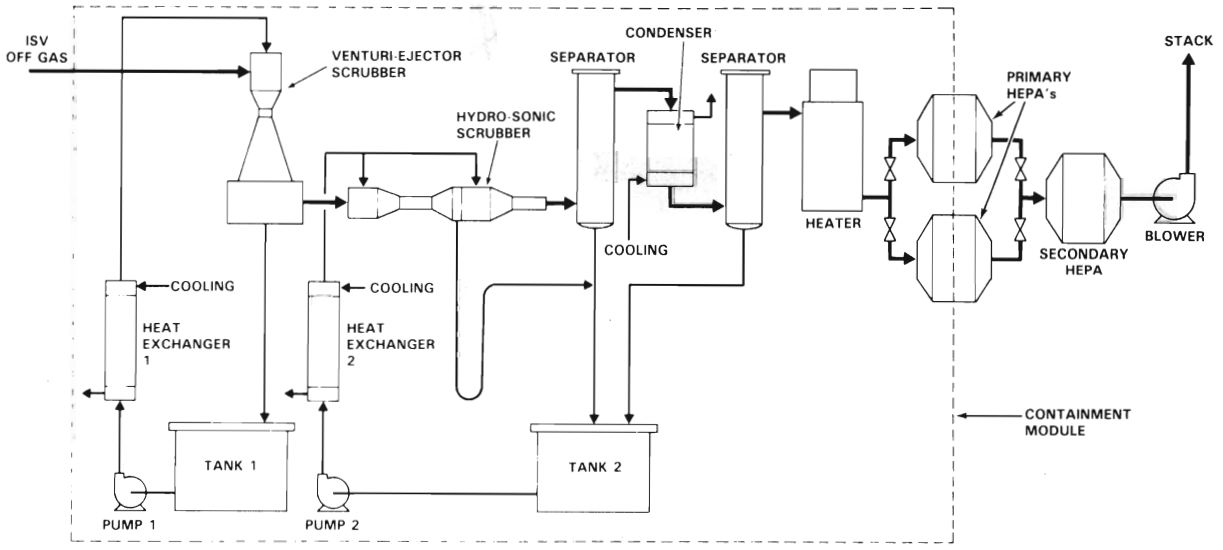

FIGURE 6. Off-Gas System Schematic for the Pilot-Scale ISV Process

® Hydro-Sonic scrubber is a product of Hydro Sonic Systems, Dallas, Texas.

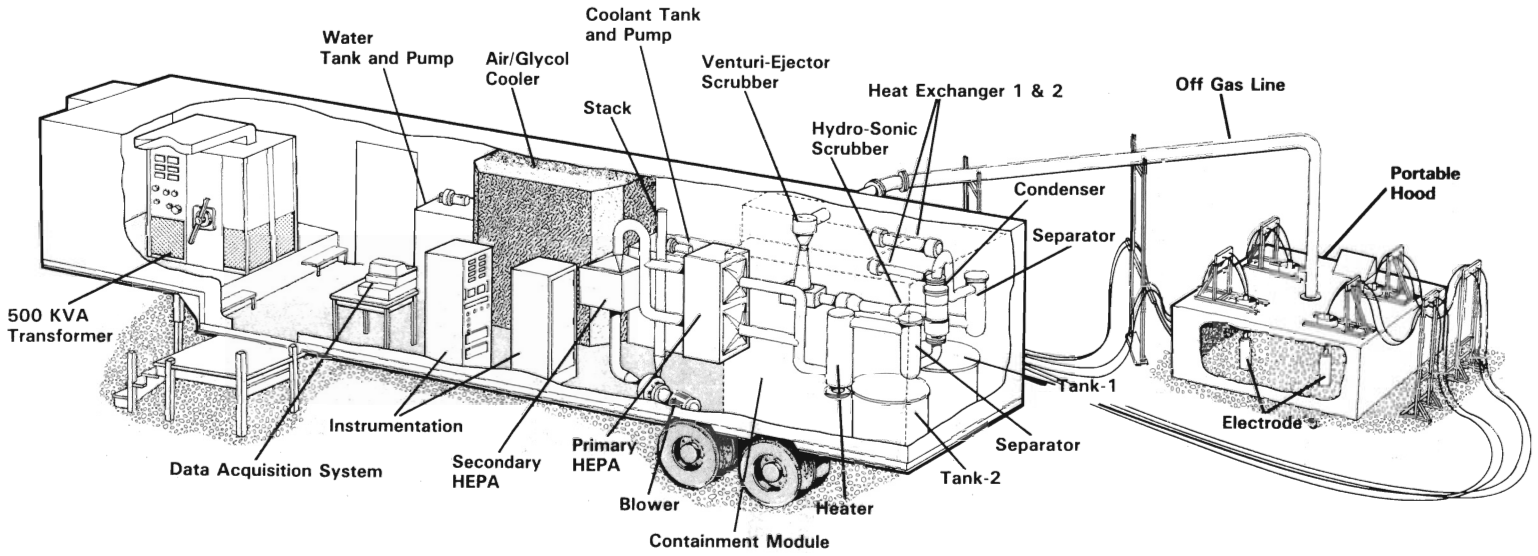

FIGURE 7. Cutaway View of Pilot-Scale ISV Process Trailer and Hood

FIGURE 8. Removable Containment Module for the Off-Gas Treatment System

The venturi-ejector scrubber serves both as a quencher and high energy scrubber. The second scrubber is a two stage Hydro-Sonic scrubber (tandem nozzle fan drive) as illustrated in Figure 9. The first section condenses vapors, removes larger particles, and initiates growth of the finer particles so that they are more easily captured in the second stage. Particulate is captured when the gas is mixed with fine water droplets produced by spraying water into the exhaust of the subsonic nozzle. Mixing and droplet growth continue down the length of the mixing tube. Large droplets containing the particulate are then removed by a vane separator and drained back into the scrub tank. The unit is designed to remove over 90% of all particulates greater than 0.5 μm dia when operated at a differential pressure of 127 cm (50 in.) water. Efficiency increases with an increase in pressure differential.

Additional water is removed from the gas system by a condenser having a heat exchange area of 8.9 m^2 (96 ft^2) and a final separator. The gases are then reheated ~25°C in a 30 kW heater to prevent condensate carryover to the filters.

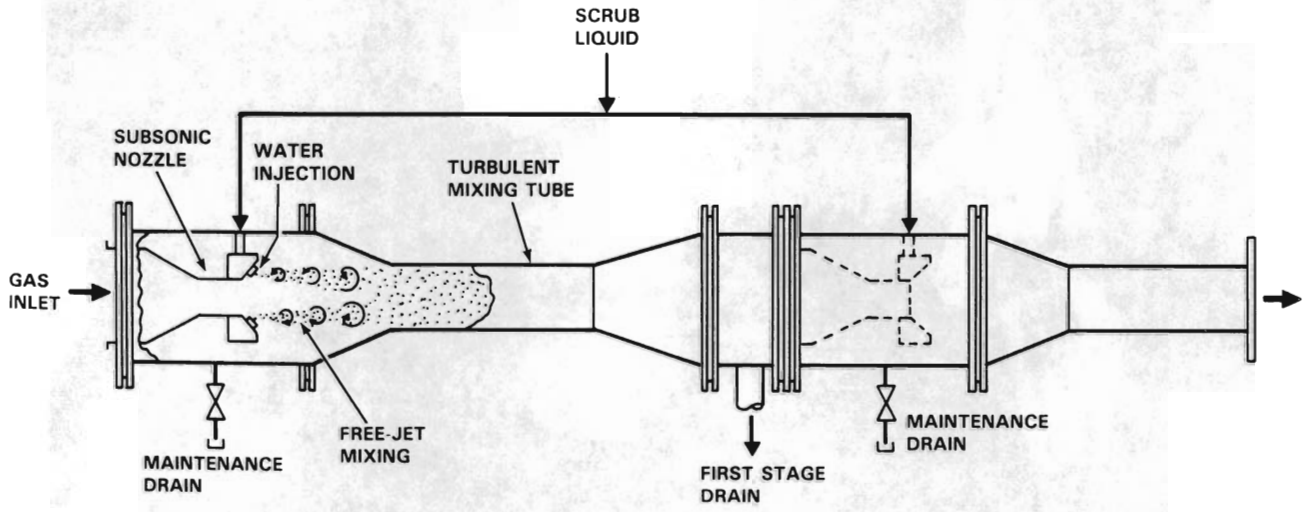

FIGURE 9. Tandem Nozzle Hydro-Sonic Scrubber (Hydro Sonic Systems, Dallas, Texas)

The first stage of filtration consists of two 61 x 61 x 29 cm (24 x 24 x 11.5 in.) HEPA filters in parallel. During operation, one filter is used and the other remains as a backup in case the generating filter becomes loaded. The primary filter can be changed out during operation. The second stage HEPA filter acts as a backup in case a first stage filter fails.

TEST DESCRIPTION

The primary objective of the radioactive test was to demonstrate the ISV processing containment and confinement of radioactively contaminated soil and to evaluate the off-gas behavior of volatile or entrained radionuclides. Prior to the radioactive test, two nonradioactive operational acceptance tests were performed. Each of these tests was configured to simulate the radioactive test, as illustrated in Figure 10. Four graphite electrodes were used with a 1.22 x 1.22 m separation. The first cold test used a metal waste container while the second cold test and radioactive test used a plastic container. The plastic container was selected for the radioactive test to minimize the possibility of a pressurized sealed container (Oma et al. 1983). Both nonradioactive tests provided operator training and equipment checkout for the system. Operational problems encountered in the first test necessitated further system check-out in the second test. The problems that were identified and resolved are highlighted below.

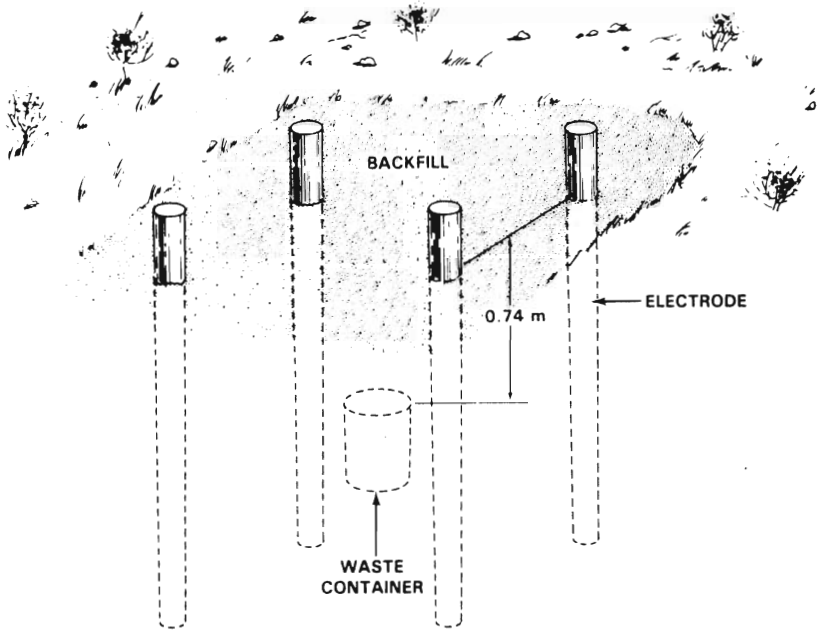

FIGURE 10. Waste Container Placement Before Vitrification

- Hood vacuum was reduced due to the drying and sloughing of the soil around the hood. A high temperature skirting was attached to the bottom of the hood perimeter to maintain the vacuum if subsidence occurred.
- Transformer phasing problems plus thermal and current trips interrupted power to the electrodes. The phasing was corrected and the current limiter was adjusted to allow the power control system to operate within safe bounds. An improvement to the transformer cooling fan shrouding enhanced the air flow across the transformer heat sink and improved the heat transfer from the transformer to prevent thermal trips.
- The temperature limits for the blower inlet did not allow enough thermal energy from the heater to evaporate all the moisture in the gas stream. Water was found on the first stage HEPA filter due to collection of unevaporated scrub solution mist from the system.
- A blower capable of higher temperature operation was installed to allow a higher temperature setting of the off-gas heater and a greater evaporation rate.

The results of the second cold test confirmed that the corrective action was satisfactory.

The ISV pilot-scale radioactive test was conducted using a make-up site, in which known quantities of radionuclides are introduced. A noncontaminated site south of the 300 West Burial Ground #7 at Hanford was chosen so an assessment of radionuclide distribution within the vitrification zone and a determination of any migration beyond the vitrification region into clean soil could be made. The radioactive material, listed in Table 2, was placed in a 19 L (5 gal) container and was centrally positioned within the zone to be vitrified (see Figure 10). The radionuclide content chosen for the test was based on the detection capability of the radiochemical analytical equipment. These detection limits were used to establish the minimum input amount for each radionuclide based on predicted losses to the off-gas system and predicted distribution within the vitrified block.

TABLE 2. Waste Container Radionuclide Inventory

Radionuclide	Total Curies	Original Concentration nCi/g
^{241}Am	0.0095	370
^{239}Pu	0.0053	210
^{238}Pu	0.0018	70
^{137}Cs	0.020	780
^{106}Ru	0.021	820
^{90}Sr	0.680	26600
^{60}Co	0.010	390

The radioactive test was successful in containing the radioactive material through the encapsulation of over 99% of the material in the melt zone and containment of the balance within the off-gas system. No release of radioactive material to the environment was detected during the actual processing operations (23 h) or during the hood plenum cool down period (30 h). The two nonradioactive runs proved to be valuable acceptance testing of the system. Analysis of the ISV system performance is tied to certain run events, such as voltage tap changes and other changes in processing conditions which could affect interpretation of the data. Table 3 lists test events and their time of occurrence. Specific equipment performance and testing results of the radioactive test and their relation to these run events are presented in the following section.

TABLE 3. Chronological List of Events During the Radioactive Test

Run Time (hr)	Event Description
0	START-UP: Power transformer at 1000 V tap
0.1	Switched from voltage to current control
1.1	Reached maximum power on 1000 V tap
1.6	Melt zone center-line depth at 1'
1.8	Gas release from waste package
2.8	Power transformer switched to 650 V tap
3.1	Reached maximum power on 650 V tap
3.3	Melt zone at top of waste package (2.5')
6.2	Added fresh water to venturi-ejector scrub tank
6.6	Power transformer switched to 430 V tap
8.3	Reached maximum power on 430 V tap
8.8	Melt zone at bottom of waste package (3.5')
10.3	Added fresh water to venturi-ejector scrub tank
13.4	Melt zone at 4' depth
19.9	Transferred a portion of the Hydro-Sonic scrub solution to venturi-ejector scrub tank
23.2	POWER TURNED OFF
25.1	Venturi-ejector scrub pump turned off
30.0	Hydro-Sonic scrubber liquid flow reduced

TEST RESULTS AND PERFORMANCE ANALYSIS

Performance of the ISV process is based on the equipment operation and the ability of the system to stabilize and contain all radionuclides added to the soil. Three primary areas of performance are addressed: 1) power system, 2) off-gas system, and 3) product characterization. Sampling positions relating to the radionuclide distribution and analysis of the off-gas system and waste form are illustrated in Figure 11.

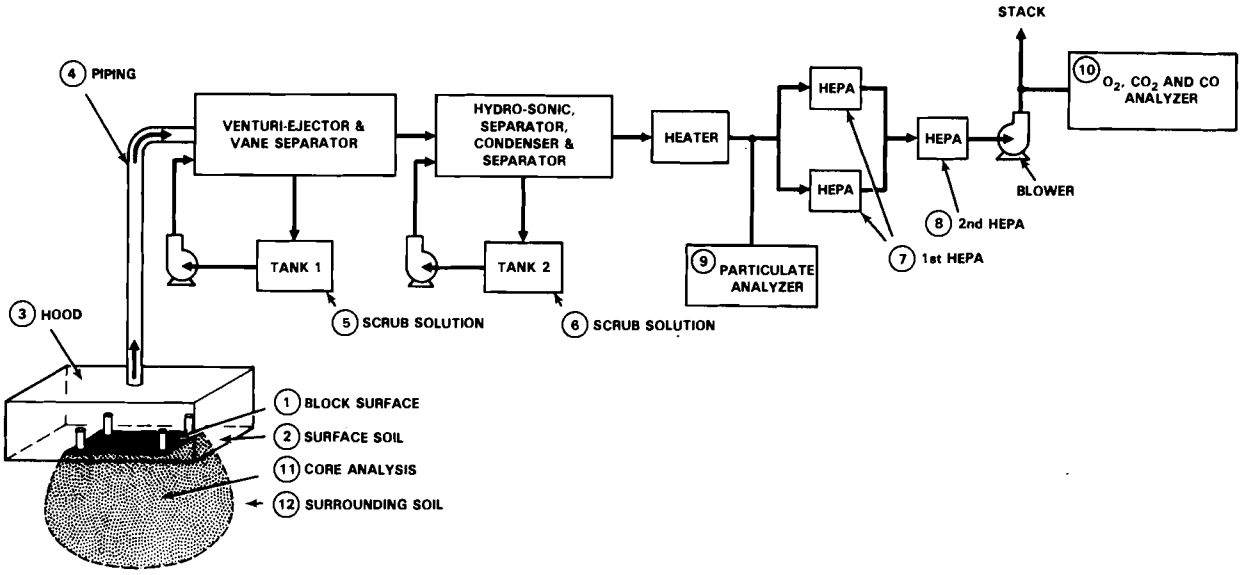

FIGURE 11. Pilot-Scale System with the Associated Sampling Positions

POWER SYSTEM

The power system performed adequately during both acceptance tests and the radioactive test. Several minor problems (incorrect phasing, current limitations, transformer thermal trips, and system amperage limitations), identified in the test description section, were resolved by correcting the phasing, adjusting the current limiter, improving the cooling air flow across the transformer heat sink, and limiting process operations to a 600 ampere maximum current load. Once all these power control system "bugs" were identified and resolved, the Scott-Tee transformer system performed to expectations, providing

a balanced supply of power to the melt. Power, voltage, and amperage performance data for the radioactive test are illustrated in Figures 12 and 13.

A power system performance comparison among the two cold tests and one radioactive test is presented in Table 4. This comparison illustrates the

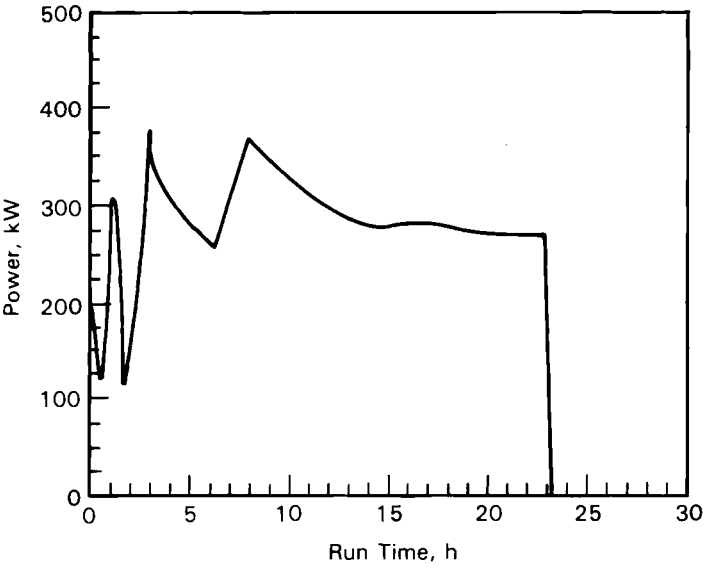

FIGURE 12. Power to Electrode

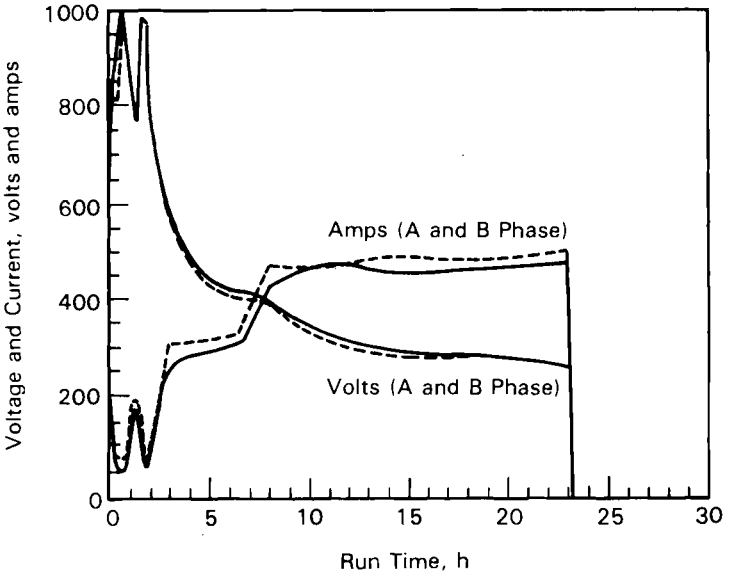

FIGURE 13. Voltage and Current

TABLE 4. Comparison of Power System Performance of Three Pilot-Scale Tests

Parameter	PSCT 1	PSCT 2	PSRT
Processing time, h	36	27	23
Soil solidified, kg	9270	8910	8600[a]
Approximate dimensions of solidification zone, m	1.8 x 1.8 x 1.5	1.8 x 1.8 x 1.4	1.8 x 1.8 x 1.5[a]
Approximate volume of solidification zone, m^3	4.9	4.5	4.9[a]
Total energy consumed, kWh	9920	8500	6900
Average power, kW	275	315	300
Maximum power, kW	410	410	375
Energy/mass, kWh/kg	1.07	0.95	0.80[a]

(a) Estimated (block still in the ground).

effects of operating condition on melting efficiency (energy/mass ratio). The energy/mass ratio from the first cold test (PSCT 1) was higher than for previous pilot-scale tests because the soil moisture was greater and the power supply system was not operating under optimum conditions (current limitations and transformer trips). The energy/mass ratio during the second cold test (PSCT 2) was also slightly higher, due to 3 hours of downtime as a result of blown fuses. When the system operated without interruptions, as was the case in the radioactive test (PSRT), an improved power efficiency (0.8 kWh/kg) was achieved, which is comparable with previous pilot-scale test operations (Timmerman et al. 1983).

OFF-GAS SYSTEM

During the radioactive test, the equipment performance was monitored by the extensive use of field instrumentation. All temperatures, pressures, flows, gas compositions, and tank levels were recorded at 6 minute intervals by

a computer controlled data acquisition unit. Data pertaining to performance of the equipment, removal efficiency of radionuclides and removal efficiency of particulate are presented below.

Off-Gas Containment Hood

The hood covering the vitrification zone maintained a slight vacuum over the molten area most of the time during the first cold test and at all times during the remaining two tests. Brief moments of reduced vacuum were experienced when the dirt seal around the base of the hood dried and partially subsided during the first cold test. A skirting made of high-temperature resistant cloth effectively eliminated the effects of soil subsidence on the hood vacuum in the other two tests.

Structurally, the hood maintained its integrity through all the tests. The pilot-scale hood was designed to withstand an 18 cm (7 in.) water vacuum. A HEPA filtered air inlet system with a slide valve was installed on the hood to insure that the plenum vacuum never exceeded the hood's structural limitations.

The hood plenum vacuum averaged between 2.5 and 4.0 cm (1.0 and 1.6 in.) water column (W.C.) during the radioactive test as shown in Figure 14. The vacuum decreased to 1.3 cm (0.5 in.) W.C. for a 10 to 15 minute period at 1.8 hours into the test when the waste package gas release was observed; however, this vacuum was still within the desired safe operating range of the hood. The gas release associated with the vacuum decrease could be attributed to one or both of the following factors: (1) air present in the double plastic bag containing the waste container expanded with heating then released suddenly and (2) thermal destruction of the plastic bags and the waste container may have resulted in a pyrolysis/combustible gas release. The remainder of the test presented no operational problems to the off-gas system through the 23 h test duration. At 30 hours after startup (7 hours after completion of the test), the liquid flow to the Hydro-Sonic scrubber was reduced, which in turn lowered the differential pressure across the off-gas system, increasing the off-gas flow and the hood vacuum (see Figures 14 and 15).

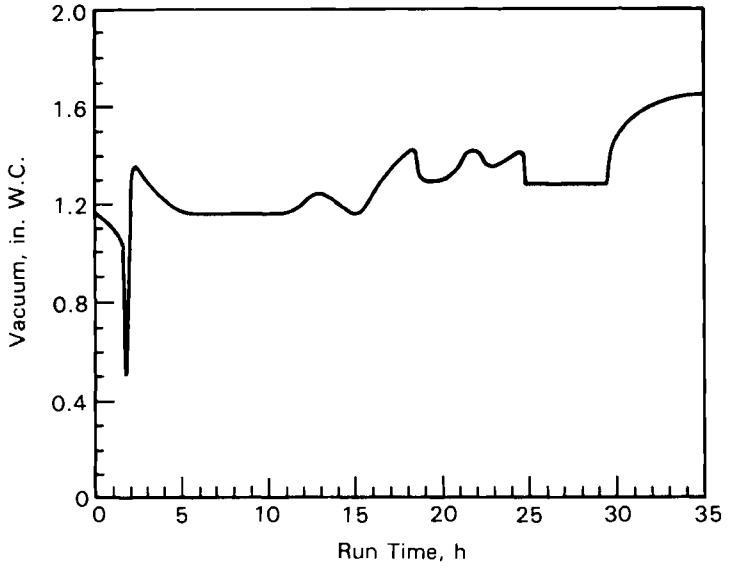

FIGURE 14. Hood Vacuum

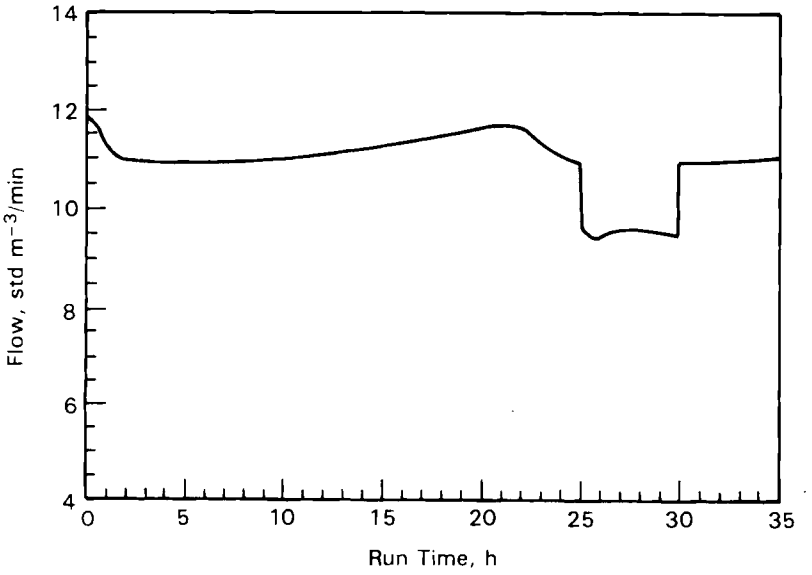

FIGURE 15. Off-Gas Flow Rate

Heat related stresses created small cracks in the hood during the first cold test one in the region directly above the melt zone. These cracks were repaired and a radiative heat shield was installed over the central region of the hood which substantially reduced thermal stress in the metal hood. Radioactive test off-gas temperatures from the hood plenum to the process trailer

are presented in Figure 16. The hood plenum temperature ranged from 300 to 360°C later in the test, essentially the same as seen in the two previous operational tests. The hood maintained its integrity and showed no weak points due to stresses imposed by thermal cycling or the vacuum. The temperature of the hood metal itself did not exceed 280°C (see Figure 17).

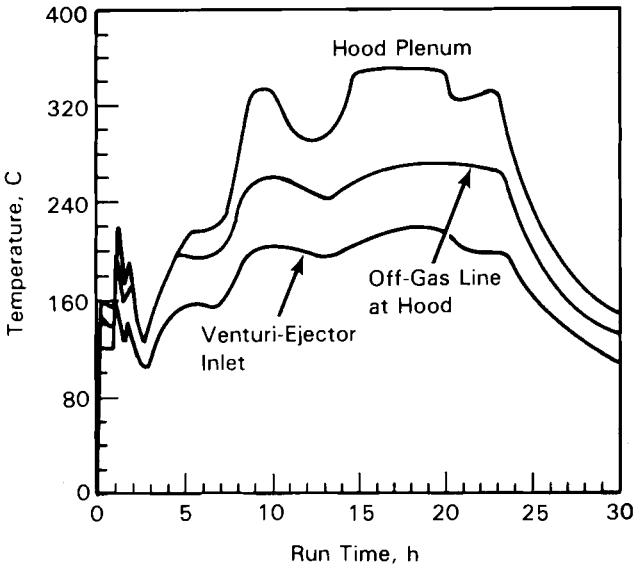

FIGURE 16. Off-Gas Temperatures from Hood Plenum to the Process Trailer

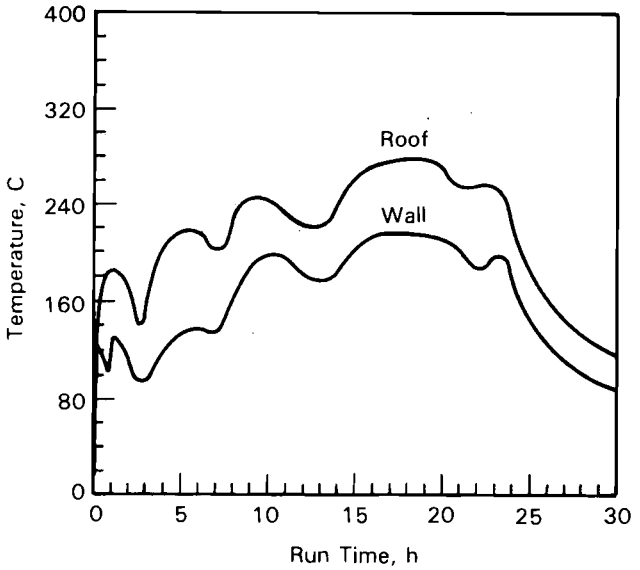

FIGURE 17. Off-Gas Hood Temperatures

The hood effectively contained off gases from the melt and supported the electrodes under varying thermal conditions. This effective containment was highlighted and proven in the radioactive test, in which no airborne radioactive contaminants were detected outside the off-gas hood.

Off-Gas Treatment Equipment

Off gases entering the off-gas system were ~60°C cooler than when exiting the hood (Figure 16) due to heat losses during flow through the off-gas line. Gas temperatures ranged from 180 to 220°C at the venturi-ejector scrubber inlet. The venturi-ejector effectively quenched them to less than 40°C. Figures 18 and 19 present the off-gas temperatures during the radioactive test at positions in the off-gas system from the venturi-ejector scrubber to the stack. Fluctuations in the temperatures within the scrub system were influenced by the ambient temperature, which determined the temperature of the water/glycol coolant. The minor effect of the day/night temperature cycle can be clearly seen from the ambient air curves of Figures 18 and 19. As seen in Figure 18, the Hydro-Sonic scrubber and condenser both cooled the gases an additional increment. The approach temperature between ambient and the condenser outlet averaged 5°C, which indicates an effective cooling system

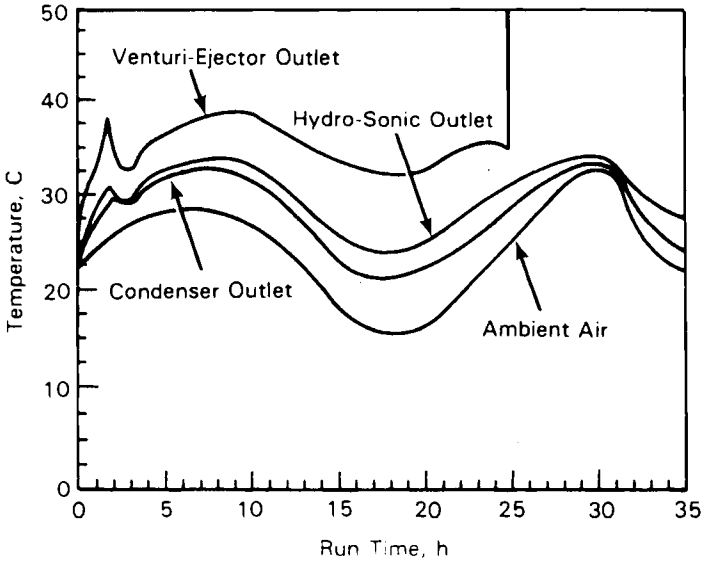

FIGURE 18. Off-Gas Temperatures from the Venturi-Ejector Outlet to the Condenser Outlet

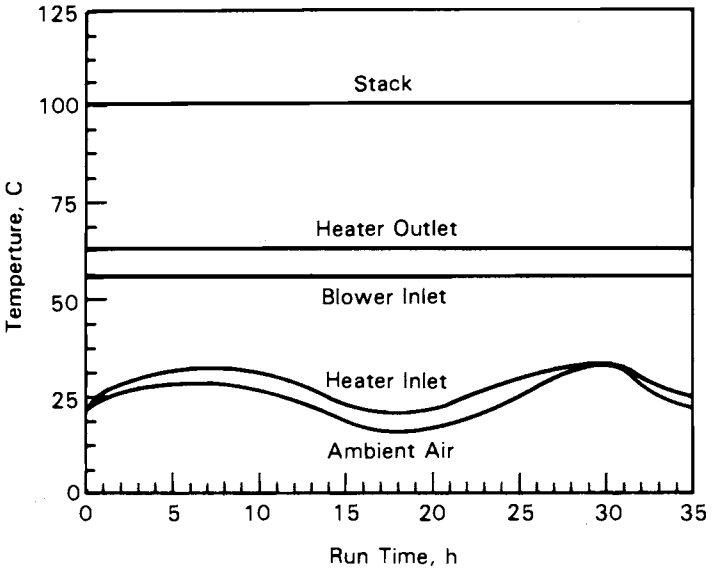

FIGURE 19. Off-Gas Temperatures from the Heater Inlet to the Stack

efficiency. After exiting the condenser, the off-gas stream was reheated to 62°C to evaporate entrained moisture before reaching the HEPA filters. The differential temperature across the heater averaged 29°C during the test. The adiabatic heating effect of the blower is apparent from Figure 19 since the off gases were heated ~45°C by the blower.

The HEPA filters gave no indication of increased flow resistance resulting from particulate loading, as indicated by differential pressure data (see Figure 20). The differential pressures averaged 2.5 cm W.C. across the HEPAs during power-on operation and fluctuated somewhat after 25 hours in response to variations in off-gas flow (Figure 15) caused by scrubber parameter changes listed earlier in Table 3.

Scrub solution was gradually carried over from the venturi-ejector scrub tank to the Hydro-Sonic scrub tank due to evaporation followed by recondensation. This effect as well as the effects of tank to tank liquid transfers (listed in Table 3) can be seen in Figure 21.

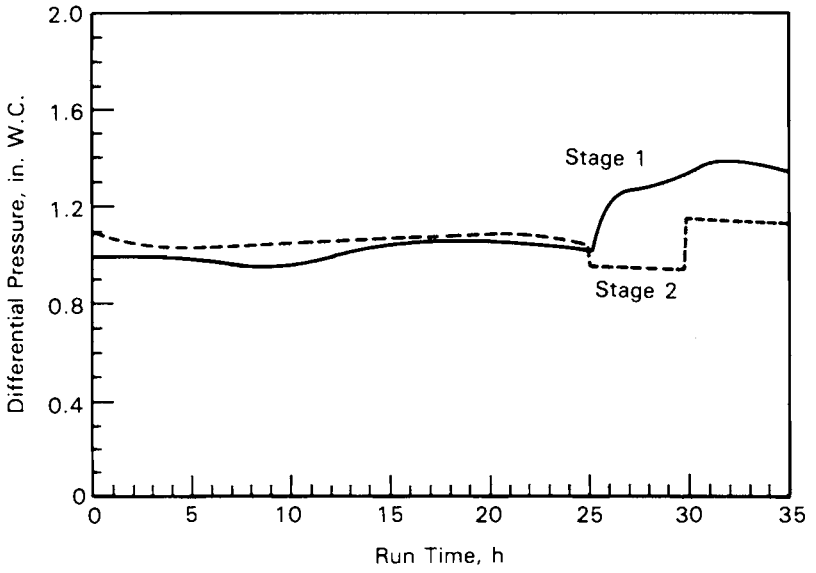

FIGURE 20. HEPA Filter Differential Pressures

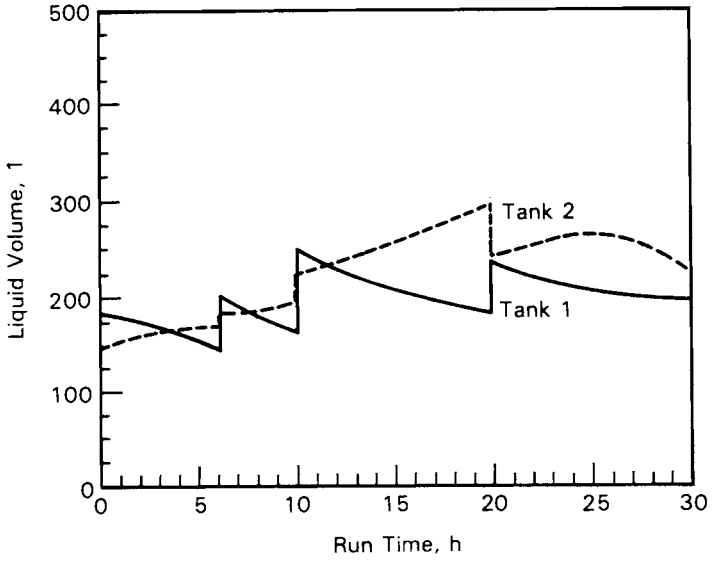

FIGURE 21. Scrub Tank Liquid Volumes

Decontamination Factors

Soil-to-off-gas decontamination factors (DFs)[a] were calculated from alpha, beta, and gamma analysis of samples taken from points 1 through 8 in the ISV system (see Figure 11). Radiochemical analytical procedures are described in Appendix A. The scrub solution was sampled periodically during the test. Samples of the block surface (smearable), surface soil, hood, piping and HEPA filters were taken during the post-run analysis period. The analytical results, calculated from the sampling data are presented in Table 5.

Table 6 shows the melt retention, percent release and soil-to-off-gas DF for the radionuclides in the test. Retention of all radionuclides by the vitrified material was greater than 99%. Decontamination factors for transuranic elements averaged greater than 4000. Fission product DFs ranged from 130 for the more volatile ^{137}Cs to 3100 for ^{90}Sr.

Off-gas releases of the more volatile fission products (^{137}Cs, ^{106}Ru, and ^{60}Co) are a function of gas releases as the melt passes through the contaminated soil and of the relative volatility of each radionuclide. Data also show that once the waste associated with these radionuclides has been vitrified, radionuclide releases to the off-gas system are relatively minor. The releases of ^{137}Cs, ^{106}Ru, and ^{60}Co from the molten soil to the hood area, piping, scrubbers, and HEPA filter are presented as a function of run time in Figure 22. Low quantities of each radionuclide began to appear in the first scrub samples at 2.1 hours into the run. The melt zone reached the bottom of the container at approximately nine hours into the test. Once the radionuclides were incorporated into the molten soil, the element releases began to slow down as depicted by the reduced slope of the Figure 22 curves. The curves indicate that the release rate is highest when the waste material is being actively melted. The higher release rate to the off gas during melting of the waste container can be attributed to combustion of the container and the thermal reaction of the radionuclides from a nitrate to an oxide form. It is expected that gases released during these reactions increase entrainment of particles and create a more direct pathway to the surface for release of the

(a) DF = reciprocal of the fraction of material released.

TABLE 5. Radionuclide Distribution within the Off-Gas System

Ci	^{241}Am	$^{239/240}Pu$	^{238}Pu	Total Pu
Original	9.5 E-3	5.3 E-3	1.8 E-3	7.1 E-3
1. Block surface	2.6 E-8	4.2 E-10	1.6 E-10	5.8 E-10
2. Surface soil	6.3 E-10	2.6 E-10	1.7 E-10	4.3 E-10
3. Hood	1.8 E-7	5.4 E-8	1.7 E-8	7.1 E-8
4. Piping	7.0 E-8	9.6 E-9	3.0 E-8	4.0 E-8
5. Venturi (Tk 1)	5.2 E-7	1.1 E-6	3.6 E-7	1.4 E-6
6. Hydro Sonic (Tk 2)	4.4 E-9	3.3 E-8	1.0 E-8	4.4 E-8
7. Primary HEPA	(a)	1.1 E-8	3.6 E-9	1.5 E-8
8. Secondary HEPA	(b)	(b)	(b)	(b)

Ci	^{137}Cs	^{106}Ru	^{90}Sr	^{60}Co
Original	2.0 E-2	2.1 E-2	6.8 E-1	1.0 E-2
1. Block surface	2.5 E-7	9.7 E-8	9.5 E-8	2.5 E-8
2. Surface soil	1.3 E-8	5.5 E-9	7.0 E-9	9.1 E-10
3. Hood	2.6 E-6	3.2 E-6	9.5 E-6	1.7 E-7
4. Piping	7.1 E-6	4.3 E-7	7.4 E-6	7.8 E-7
5. Venturi (Tk 1)	2.7 E-5	9.3 E-6	1.9 E-4	1.3 E-6
6. Hydro Sonic (Tk 2)	1.1 E-4	2.4 E-5	9.3 E-6	3.0 E-6
7. Primary HEPA	5.0 E-6	1.1 E-6	2.3 E-7	1.8 E-7
8. Secondary HEPA	<1.0 E-9(a)	<2.2 E-8(a)	(b)	<3.6 E-9(a)

(a) Not detected. Values shown are based on analytical detection limits.
(b) Analysis of these nonvolatile species was not performed.

more volatile elements. This effect was seen to a greater extent during previous pilot-scale tests with combustibles and chemical nitrates (Oma, Farnsworth, and Timmerman 1984). The relative volatility of each radionuclide is also represented in Figure 22 by the range of the releases, with Cs being the most volatile and Co exhibiting the lower release potential.

TABLE 6. Radionuclide Release Data

Radionuclide	Melt Retention, %	Release to Off Gas, %	Soil-to-Off-Gas DF
(transuranics)			
Am-241	99.992	0.008	12,000
Pu-239/240	99.977	0.023	4,300
Pu-238	99.978	0.022	4,500
Total Pu	99.978	0.022	4,500
(fission products)			
Cs-137	99.23	0.77	130
Ru-106	99.82	0.18	550
Sr-90	99.968	0.032	3,100
Co-60	99.945	0.055	1,800

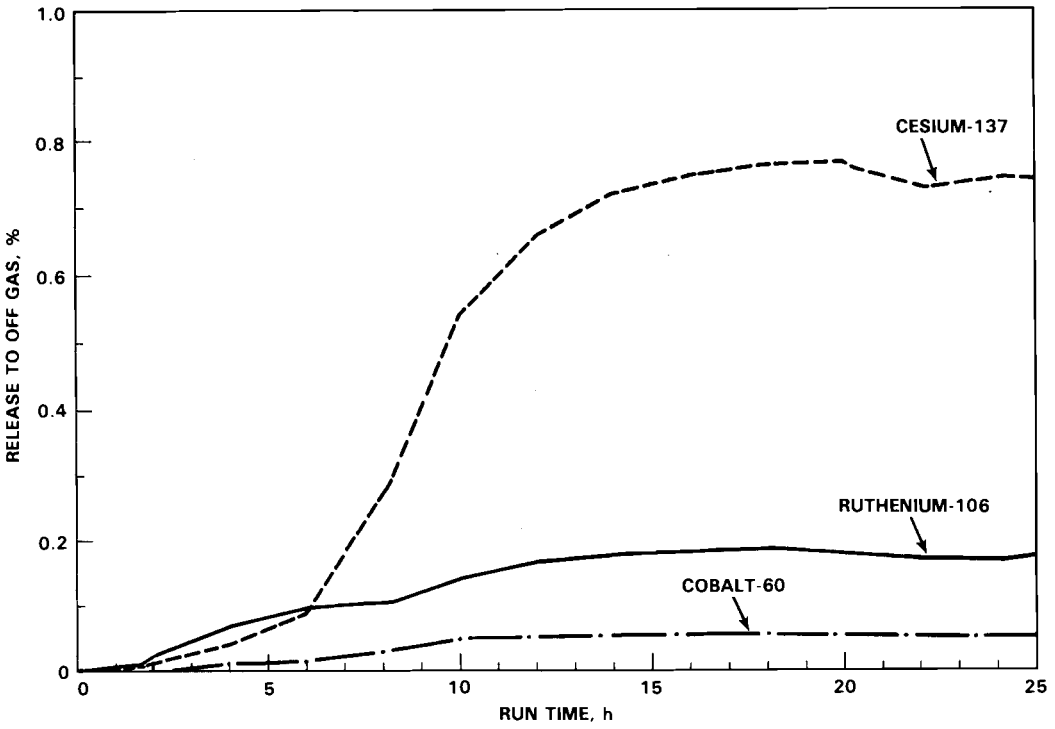

FIGURE 22. Cesium, Ruthenium and Cobalt Released to the Off-Gas System

Releases of nonvolatile components (Pu and Sr) occur primarily when the melt zone initially contacts the contaminated zone, causing a gas release

associated with vitrifying gas-generating wastes such as combustibles or nitrates. Plutonium and strontium releases both peaked 4 hours into the run as shown in Figure 23 and appeared to decrease to a steady value later in the test. This apparent decrease (approximately a factor of 2) is not real. In fact, the total radionuclides collected in the off-gas system increased slightly. Release projections extrapolated from previous data (Oma, Farnsworth, and Timmerman 1984) are illustrated in Figure 24. The earlier projections show the typical trend of an initial element release associated with gas generation and then little or no further release throughout the remainder of the test.

The decrease in release with time indicated in Figure 23 is apparently caused by a decrease in the leaching efficiency of the extractive chemistry technique applied to the solid phase residue and used to separate and analyze these radionuclides. A similar leaching extraction is used for both the Pu and Sr. This technique was not adequate to remove these elements from the solid phase prior to the alpha and beta counting. When leachates from the same

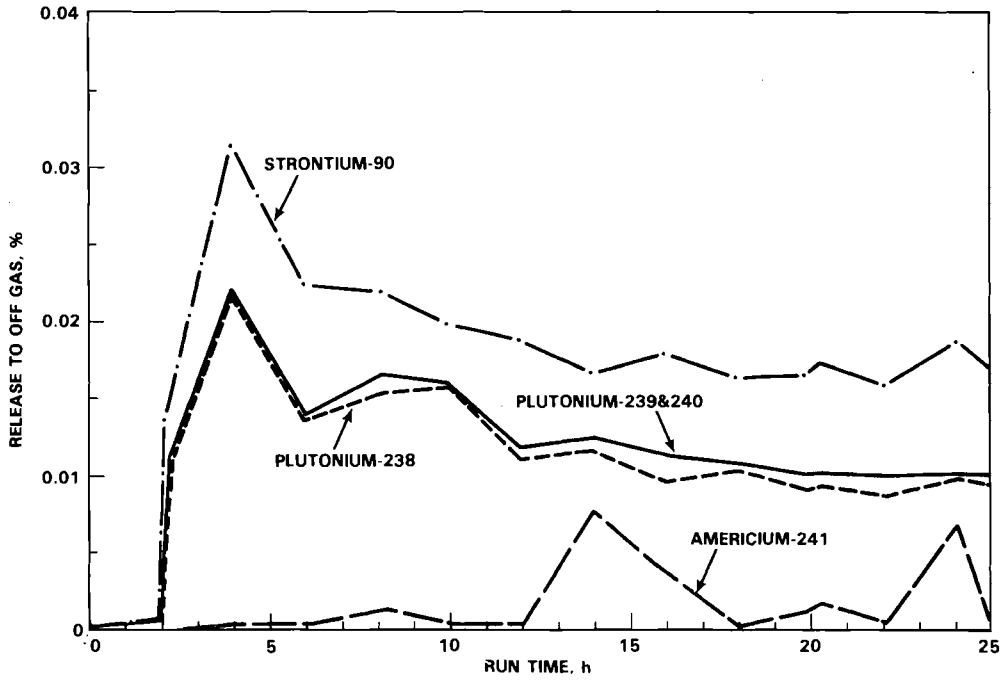

FIGURE 23. Americium, Plutonium and Strontium Released to the Off-Gas System

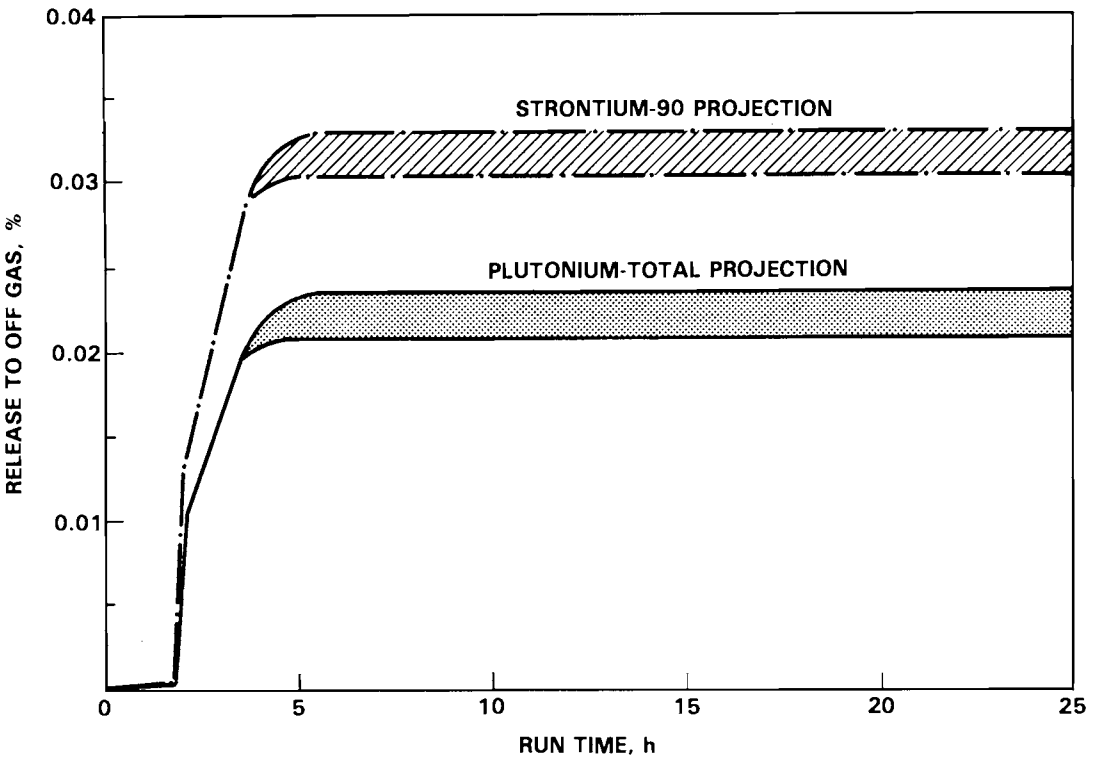

FIGURE 24. Plutonium and Strontium Release Projections

samples were analyzed for gamma emitting radionuclides, a similar decline in the measured activity occurred for samples taken later in the test, as illustrated in Figure 25. This leachate activity decline is also due to the decrease in ability to effectively leach the radionuclides from the scrub solution solid phase residue. Cesium, ruthenium, and cobalt activity decline is inconsistent with previous total sample counts of these radionuclides shown earlier in Figure 22, which illustrates that the gamma emitting radionuclides were released to some constant value later in the run and did not decline. This decline later in the test is only observed for isotopes in the solid phase. Apparently an insoluble matrix was being formed which inhibits the leaching efficiency. The liquid phase concentration of all the radionuclides showed a slight increase as a function of time which is the normal pattern. An example of the solid/liquid phase variation as a function of run time using Pu data is presented in Figure 26. Past experience in similar test conditions (Oma, Farnsworth, and Timmerman 1984) has indicated that off-gas particulates,

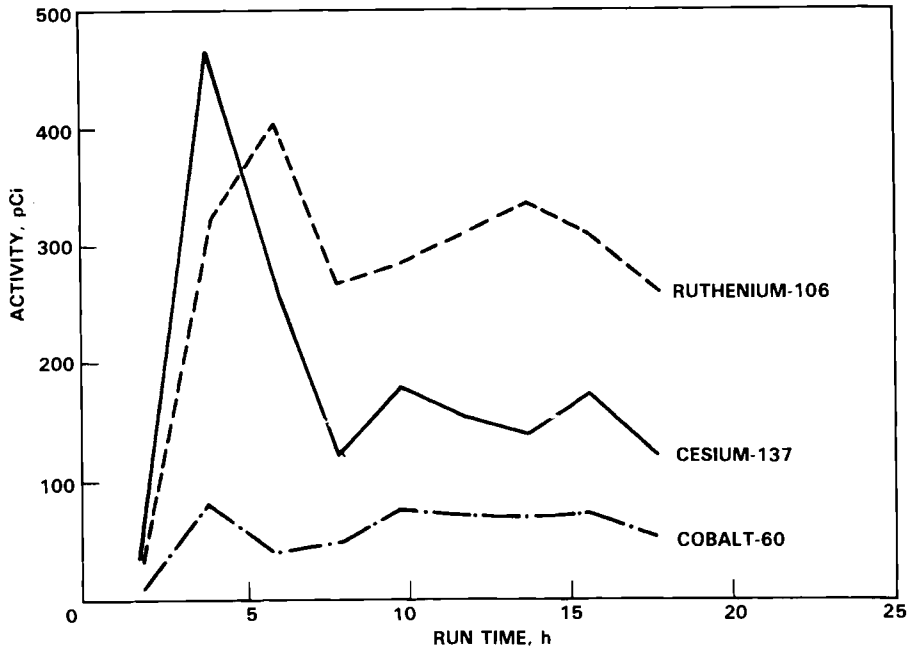

FIGURE 25. Activity in Extractive Leach Solutions of Gamma Isotopes

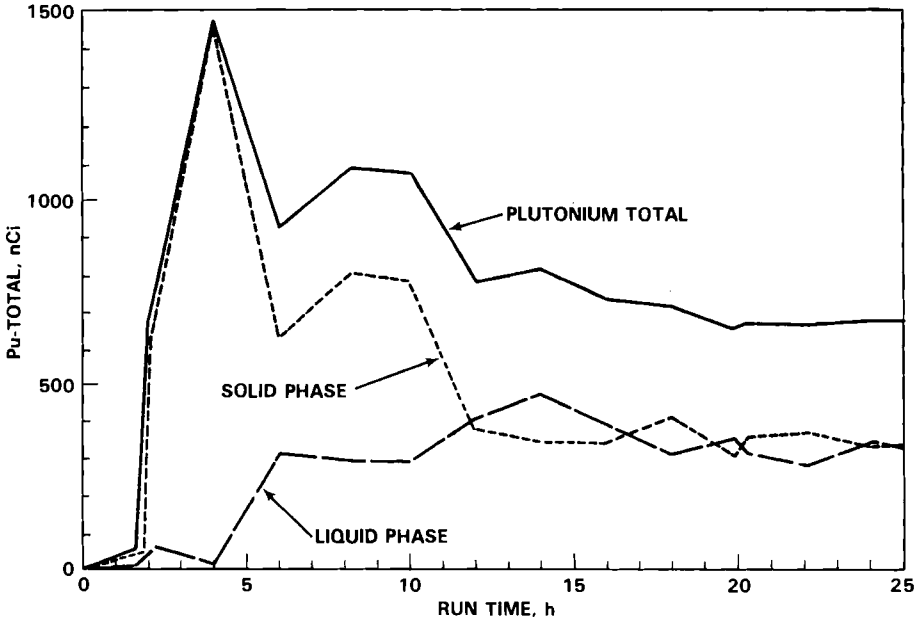

FIGURE 26. Plutonium Distribution Between Solid and Liquid Phase of Scrubber Solution

which the Pu and Sr represent, are released during the initial melt contact with the contaminated zone and are not measurably released later in the test (see projections provided in Figure 24). This initial release corresponded to the gas release (Oma et al. 1983, 1984) produced by the vitrification zone contacting the container of radioactively contaminated soil. Therefore, the peak values for these and all radionuclides were used as the total release losses to the off-gas system for this test.

Due to the extremely low activity of ^{241}Am relative to the other higher energy gamma emitting radionuclides (Cs, Co, and Ru), ^{241}Am had higher error bounds associated with its distribution measurements. Therefore, the higher errors, associated lower detectability, and higher background energy levels in the scrub solutions resulted in the more random off-gas loss curve as seen in Figure 23. However, the indicated detectable losses are relatively low.

The distribution of the radionuclides throughout the off-gas system provides insight into operational procedural requirements, projected results, scrubber efficiencies, and radionuclide particle size. Figure 27 illustrates this data. (Note: This distribution data represents only the less than 1% of

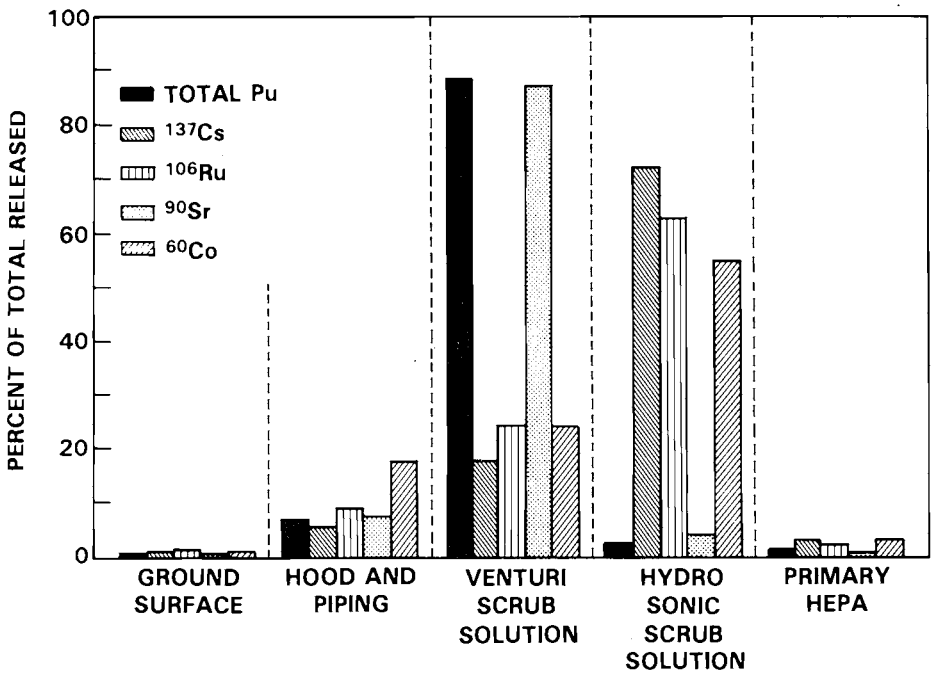

FIGURE 27. Distribution of Radionuclides Released from the Melt Zone

each radionuclide released from the melt.) As seen, only a small percentage of the elements remain on the soil and glass surface inside the hood. The scrubbers accounted for removal of from 65 to 92% of the radionuclides released as indicated by the distribution in the two scrub solutions. Based on the data, 97% or more of these radionuclides were removed from the off-gas stream prior to HEPA filtration and the balance was removed by the first stage HEPA. No gamma emitting radionuclides were detected on the second stage HEPA filter or on stack sample filters, thus demonstrating containment of radionuclides by the off-gas system. Surveys of the test site and smear samples of the outer surfaces of the hood and off-gas line were taken to verify that no releases of radionuclides took place.

Entrained particulates in the off gas exiting the ISV hood were measured during previous nonradioactive pilot-scale tests to have an average mass-mean diameter of 0.7 μm. The scrubbing efficiency of a venturi-ejector typically drops off for particles smaller than about 2 μm diameter. The hydro-sonic scrubber is more efficient since the lower limit of high efficiency is approximately 0.5 μm diameter. The distribution data between the venturi and hydro-sonic scrub solutions (Figure 27) indicate that the more volatile components, ^{137}Cs and ^{106}Ru, are being released as smaller particles since the removal by the venturi-ejector is low. Both Cs and Ru have been shown to vaporize from molten waste glasses (Gray 1980). The vapors recondense as extremely fine particles. The radionuclide distribution indicates that Co is very small also; however, the reason is not apparent from the data. Americium, plutonium, and strontium, on the other hand, were collected primarily by the venturi-ejector. This indicates that the majority of these elements were released from the melt as particles larger than 2 μm with other nonvolatile soil species. It also confirms Am, Pu, and Sr releases as particulates and assists in corroborating earlier statements relating their releases with the initial contact of the melt with the waste package.

Particulate Characteristics

During the radioactive test, particle mass loading and size distribution measurements were made at a point in the off-gas line between the heater and HEPA filters. The purpose of the measurements was to characterize the

entrained solids which were not removed by the venturi-ejector and hydro-sonic scrubbers. Data was obtained using an Active Scattering Aerosol Spectrometer Probe mounted adjacent to the off-gas line in the containment module (see Figure 11). A gas sample stream was drawn isokinetically from the off-gas line, then passed through a sheath airflow heater to prevent condensate from forming, and was injected into the measuring chamber with an aerodynamically focused jet. The particle count and size is determined by measuring the light scattering from a He-Ne laser beam passing through the focused sample stream. The probe counts the particles in four overlapping size ranges and has a useful range of 0.12 μm to 7.5 μm. The smaller size ranges have increased resolution over the larger ones, giving the probe extremely good resolution in the submicron region. Particle data is transferred from the probe to a computer controller for printing.

The entrained particle mass loading down stream of the scrubbers was extremely low during the test, averaging 0.8 mg/m^3. As seen in Figure 28, the highest loading of 2.18 mg/m^3 occurred when the graphite starter material was

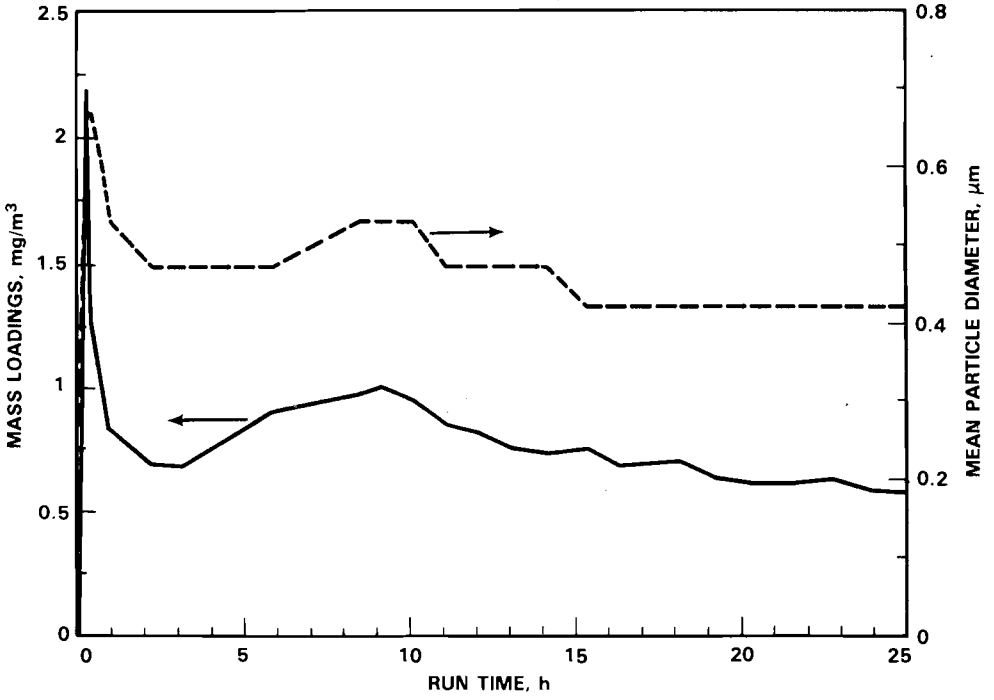

FIGURE 28. Off-Gas Particulate Mass Loading and Mass Mean Particle Diameter

actively burning. Although the off-gas particle loading at the hood was not measured during the test, it was typically greater than 1000 mg/m^3 during the start-up period of previous pilot scale tests (Oma, Farnsworth, and Timmerman 1984). As shown in Figure 28, the mass mean particle diameter averaged less than 0.5 μm (the approximate lower limit of the hydro-sonic scrubber).

Histograms of the particle mass distribution before the radioactive test (control data), during start-up, and later in the test are presented in Figure 29. The mass loading was extremely low (0.01 mg/m^3) prior to the ISV

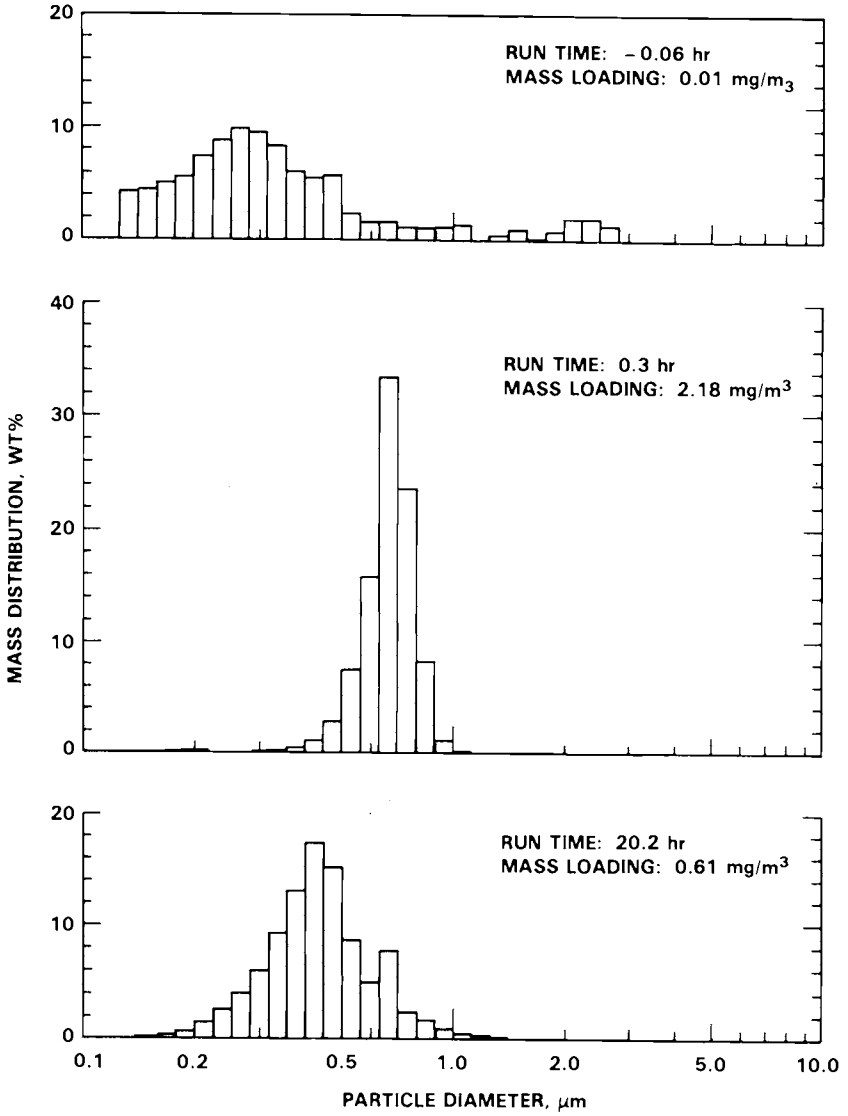

FIGURE 29. Histograms of Particle Mass Distribution

test with a distribution from less than 0.12 μm to ~2.0 μm. During startup, the mass was primarily between 0.3 and 1.0 μm. The mass distribution shifted downward later in the run but still remained above 0.2 μm. This particle size range is well within the efficient operating range of the HEPA filters.

Gaseous Characteristics

Gases were analyzed for O_2, CO, and CO_2 at a point down stream from the off-gas blower (see Figure 11). The O_2 analysis was performed by a coulometric process whereby the gas sample is passed through an electrochemical cell. Both the CO and CO_2 analysis was performed using a non-dispersive infrared monitoring technique.

Figure 30 presents the CO and CO_2 concentrations as a function of run time. The CO_2 level in the off-gas peaked at 2.25%, 1.2 hours into the test. This corresponds to the period of most active combustion of the graphite/frit startup path. This also corresponds to a period of higher power input.

The CO_2 level after the initial startup period can be explained by graphite electrode oxidation due to heating from the molten zone. Maximum power on the 650 V tap was achieved at 3.1 hours and maximum power on the 430 V tap was realized at 8.3 hours. Just prior to each of these maxima, the CO_2 levels

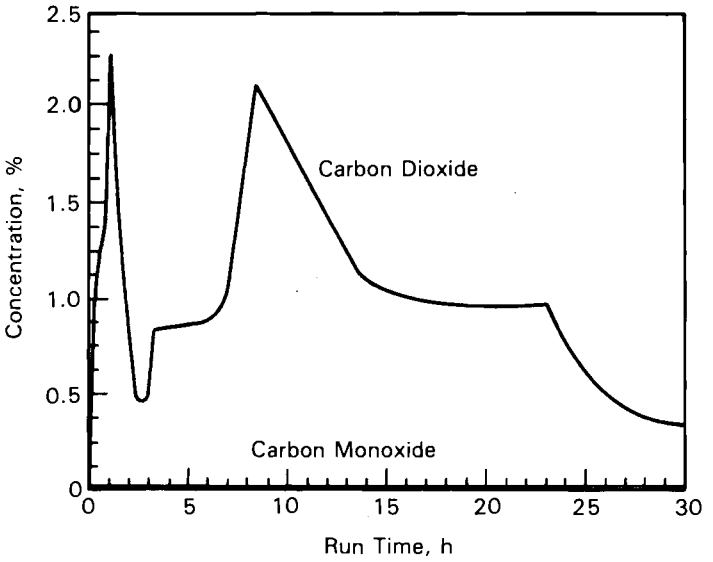

FIGURE 30. Carbon Dioxide and Carbon Monoxide Concentrations

begin climbing as the electrode oxidation rate increased. During these power maxima, the melt zone temperature increased causing the electrode to reach higher temperatures and oxidize faster. It is hypothesized that the electrode temperature at the 3.1 hour power maxima was lower than during the 8.3 hour maxima because the thermal mass of the melt zone was much smaller early in the test. The CO_2 concentration supports this, since the level was highest (excluding startup) at 2.15% during the second power maxima at 8.3 hours. As the melt continued to grow downward and the power declined, the CO_2 concentration in the off gas also decreased to approximately 1% where it remained until the power was turned off. Carbon monoxide was detected during the test, however, the concentration remained low, never exceeding 0.04% at the stack.

The O_2 concentration (Figure 31) supports this graphite oxidation mechanism since it basically mirrors the CO_2 concentration. As indicated by the O_2 concentration plot, significant combustion of the graphite startup path only occurred early in the test; with O_2 levels approaching those of atmospheric conditions in the remainder of the run.

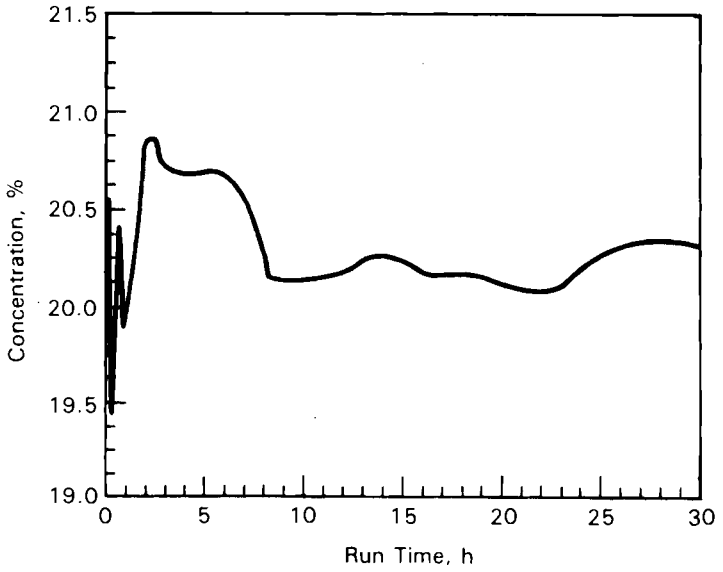

FIGURE 31. Oxygen Concentration

PRODUCT CHARACTERIZATION

This section discusses the radionuclide distribution within the vitrified block and the analysis for migration outside the block. Block sampling was accomplished by core drilling seven 5 cm (2 in.) diameter full-depth cores at locations identified in Figure 32. Migration effects beyond the block were determined from soil sampling taken directly adjacent to the vitrified mass.

Preliminary gamma scanning of all core sections as a function of depth was performed to provide an indication of the relative distribution of radionuclides throughout the block. Overall the gamma emitting radionuclides were shown to be distributed throughout the block. Selective concentrated areas were identified and will be discussed later in this section. After the preliminary analysis, core sections were ground and crushed to provide an improved geometry for the gamma scanning and to allow extractive chemistry methods to be used for Pu and Sr analysis. These analysis techniques (see Appendix A) were selectively applied to four cores (A-D). Both the preliminary and selective analytical data are presented in Appendix B. The distribution analysis between the preliminary and selective gamma analysis shows good agreement between the two analyses indicating a homogeneous distribution within samples and throughout the block.

The top and the bottom portions of the central region (Core A) are identified as concentrated areas for ruthenium and cobalt. In the case of ruthenium, similar concentrated areas near the surface and the bottom of the

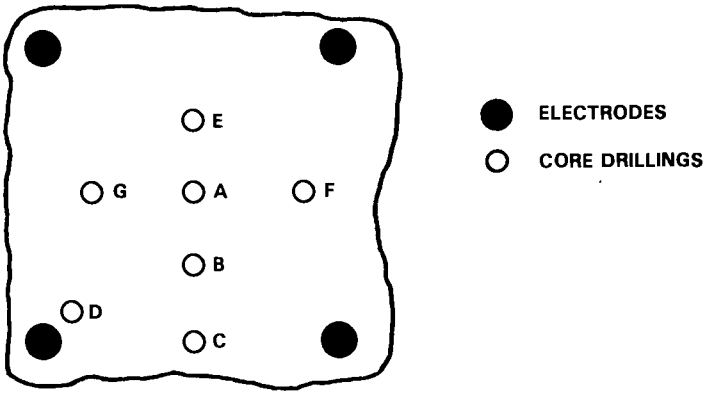

FIGURE 32. Core Drilling Positions

block were observed in most cores. A selective movement to cooler regions in the vitreous mass may be caused by the partial volatility of Ru (Gray 1980). All other radionuclides--Am, Pu, Cs, Sr, and Co (excluding Core A)--show a fairly uniform distribution in all of the core samples.

The degree of uniform distribution may be a function of the actual physical mass of material in the melt. These comparison values are illustrated in Table 7 to show this effect. Table 7 data suggests that the more inhomogeneous radionuclides (Ru and Co) also have the least mass of all radionuclides, which may affect their distribution by the convective currents during vitrification. Cobalt and ruthenium are the only radionuclides in Table 7 whose distribution standard deviations exceed the average measured value, indicating a more random distribution.

The measured distribution averages do not consistently agree with the predicted homogeneous concentration in the block as compared in Table 7. The gamma emitters agree more closely with the predicted values indicating there may be a bias associated with the Pu and Sr analytical techniques either on the original soil values used to calculate the predicted distribution or on the vitrified samples providing the measured distribution. No analytical errors were found upon reinvestigation of the data. The projected block weight could

TABLE 7. Comparison of Mass Versus Distribution of Radionuclides

Radionuclide	Mass (g)	Predicted Homogeneous Distribution (pCi/g)	Average Measured Distribution (pCi/g)	Measured Distribution Std Dev (pCi/g)
^{239}Pu	8.5×10^{-2}	620	1,460	700
^{241}Am	2.8×10^{-2}	1,100	1,300	380
^{90}Sr	5.0×10^{-3}	79,000	193,000	74,000
^{137}Cs	2.3×10^{-4}	2,300	3,500	830
^{238}Pu	1.1×10^{-4}	210	510	190
^{60}Co	8.8×10^{-6}	1,200	1,100	3,800
^{106}Ru	6.3×10^{-6}	2,400	2,600	11,000

account for a minor amount of this discrepancy; however, the main conclusion remains that the Pu and Sr data do indicate a uniform distribution of these radionuclides within the block.

Combining the preliminary and selective analytical data and utilizing the A, B, C, and E cores (Core E was not analyzed for Sr or Pu) to provide a planar profile of radionuclide distribution, Figures 33 and 34 provide these concentration distributions for transuranics and fission products, respectively. All radionuclides are distributed throughout the block which corresponds with similar distribution data from previous tests with nonradioactive chemical species (Timmerman and Lokken 1983).

The distribution profiles indicate a relatively uniform distribution for all radionuclides excluding Ru in all cores and cobalt in Core A. Plutonium and strontium data also indicate a uniform distribution. This data confirms previous indications (Oma et al. 1983) of an even distribution of Pu and allays any criticality concerns over the selective migration of Pu.

Soil samples surrounding the block were taken to determine if migration of hazardous constituents occurs beyond the vitrification zone. Five equidistant samples on the northwest face directly adjacent to the block were taken at 6 inch depth intervals from the top to the bottom of the block. Overall, the samples indicated no detectable migration of radionuclides outside the vitrification zone (see Table 8 - only selected analyses were performed for Pu and Sr). Activity was found in a few of the near surface samples; these samples were probably cross contaminated with surface soil containing radioactive material from off-gas releases. Most other soil measurements were low enough to indicate that no migration occured outside the vitrification zone (excluding any sampling errors). Referencing these low activities to natural background levels puts these levels in perspective. For example, ^{137}Cs and $^{239/240}Pu$ are naturally occurring in western surface soil at activities of 4.5 and 0.07 pCi/g, respectively (Robertson et al. 1981). As is seen from Table 8, the majority of the samples are well below the natural background levels.

The level of activity in the radioactive block was too low to obtain absolute quantitative results from an MCC-1 leach test. Projected leach quantities are three orders of magnitude below detection limits. To put the

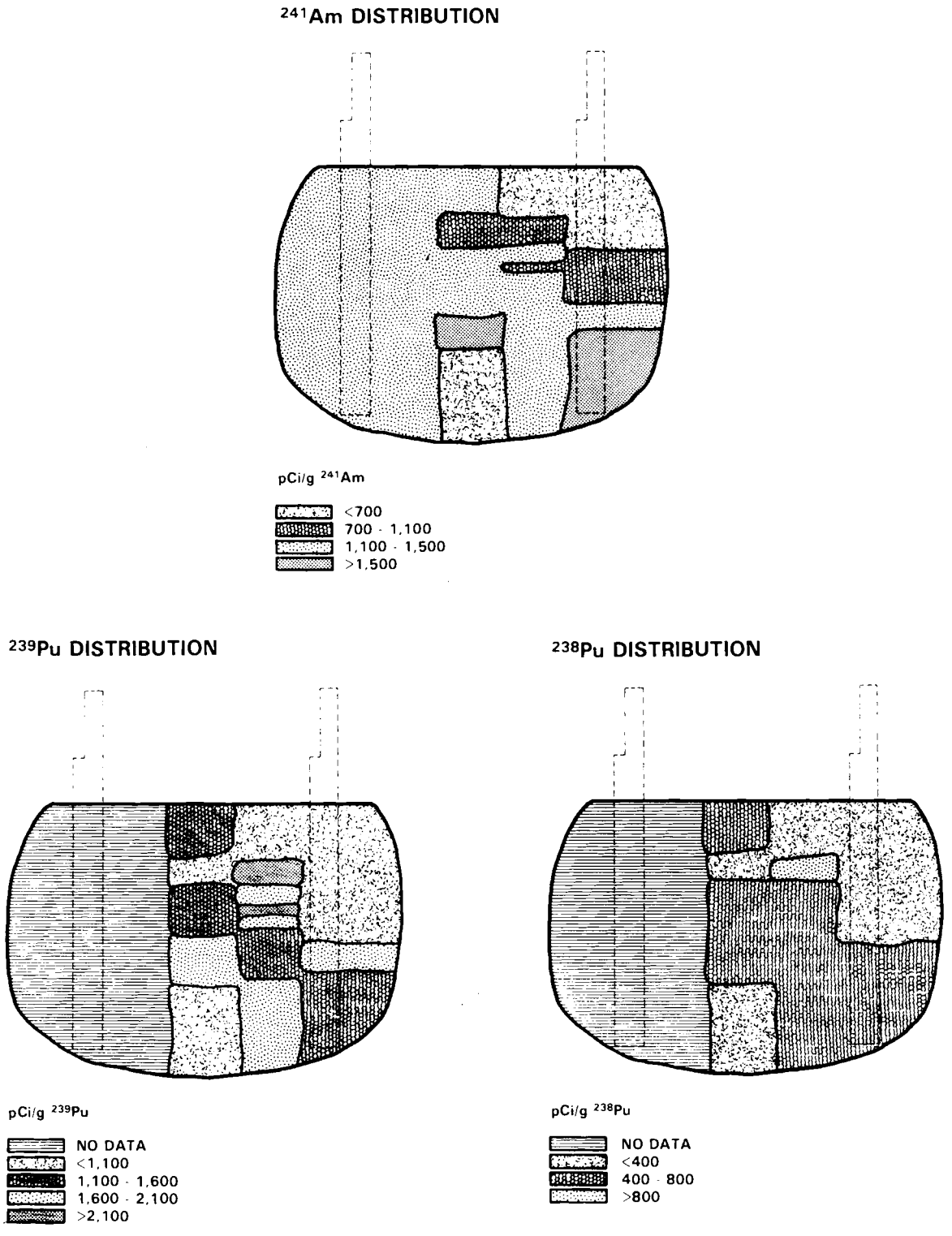

FIGURE 33. Distribution Profiles of Transuranics Radionuclides

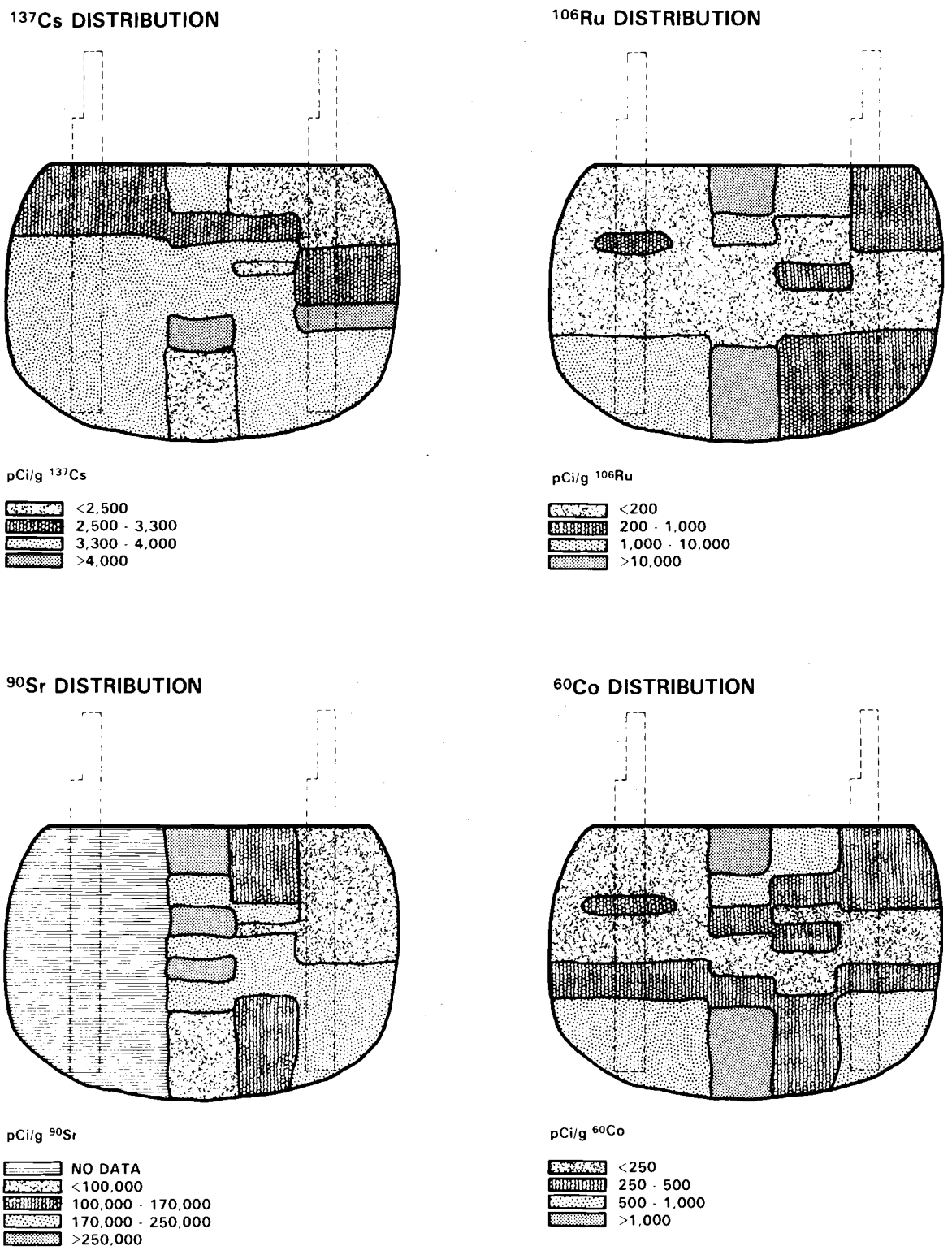

FIGURE 34. Distribution Profiles for Fission Product Radionuclides

TABLE 8. Analysis of Soil Surrounding the Vitrified Block

Depth (in)-Sample No.	(pCi/g) ^{60}Co	^{241}Am	^{137}Cs	^{106}Ru	^{238}Pu	$^{239/240}Pu$	^{90}Sr
0-1	7.5	54.9	119	5.7	0.02	0.03	<4.3
0-2	0.7	0.5	5.9	2.4			
0-3	<0.2	<0.2	1.2	<0.8			
0-4	0.3	<0.2	1.9	1.5			
0-5	4.1	4.3	51.9	21.3	0.03	0.05	<4.3
6-6	<0.2	<0.2	0.6	<0.6			
6-7	<0.2	<0.2	0.2	<0.7			
6-8	<0.2	<0.5	<0.2	<1.5	0.002	0.003	<4.1
6-9	<0.2	<0.5	1.3	<1.6			
6-10	0.2	<0.6	1.4	<2.0			
12-11	<0.2	<0.4	0.8	<1.4			
12-12	<0.2	<0.2	0.2	<0.6			
12-13	<0.2	<0.3	0.2	<0.9	0.002	0.003	<4.4
12-14	<0.2	<0.1	0.2	<0.4			
12-15	<0.2	<0.2	0.2	<0.4			
18-16	<0.2	<0.2	0.9	<0.5			
18-17	0.7	<0.2	0.2	<0.6			
18-19	<0.2	1.0	3.3	<0.6	0.01	0.05	<4.7
18-20	<0.2	<0.2	0.2	<0.5			
18-21	<0.2	<0.4	0.3	<1.2			
24-22	<0.2	<0.5	0.2	<1.2			
24-23	<0.2	<0.2	0.2	<0.5			
24-25	<0.2	<0.4	0.3	<1.2			
24-26	<0.2	<0.2	<0.1	<0.6			
30-27	<0.2	<0.7	<0.3	<2.0			
30-28	<0.2	<0.5	0.7	<1.3			
30-29	5.5	2.0	6.6	2.6	0.009	0.009	<4.5
30-30	<0.2	<0.4	<0.2	<1.2			
30-31	0.4	7.4	24.8	<2.5			
36-32	<0.2	1.4	4.3	<0.7			
36-33	<0.2	<0.6	<0.2	<1.9			
36-34	<0.2	1.5	4.7	<0.5			
36-35	<0.2	<0.2	<0.1	<0.5			
36-36	<0.3	<0.4	<0.2	<1.3			
42-37	<0.2	1.0	3.8	<0.5			
42-38	<0.2	<0.2	<0.3	<0.5			
42-39	<0.2	1.0	3.8	<0.6	0.03	0.07	<4.4
42-40	<0.2	<0.2	<0.1	<0.5			
42-41	<0.2	1.8	5.3	<0.8			

durability of the ISV product in perspective, concentrated hydrofluoric acid had to be used instead of concentrated hydrochloric acid to effectively remove enough Pu and Sr from the core samples to perform their respective analyses. Previous leach test results (Oma et al. 1983) have illustrated the impressive durability of the ISV waste form.

CONCLUSIONS

The in situ vitrification pilot-scale radioactive test has illustrated the successful stabilization of radioactive material within the vitrified soil with no release of radioactive material during operations. In addition, the test provided the following conclusions regarding ISV system performance.

- The power system performed as designed, providing an average of 300 kW of balanced two phase power to the electrode.
- No migration of radionuclides to the soil outside the vitrified mass occurred.
- All radionuclides were distributed throughout the vitrified zone, some more uniformly than others. Ruthenium and cobalt were more concentrated near the top and the bottom of the block, however, no migration into the surrounding soil occurred.
- Greater than 99% of all radionuclides were retained within the vitrified block.
- The off-gas treatment system effectively contained all radionuclides released during the test and during the cooldown period.
- Radionuclide losses to the off-gas system varied from 0.02% for Pu to 0.8% for the more volatile Cs. Corresponding DF's varied from over 4000 to 130.
- The results of this test were closely predicted by the non-radioactive series of tests, providing confidence that a radioactive test can be based upon and emulated by a valid non-radioactive test program.

REFERENCES

Brouns, R. A., J. L. Buelt, and W. F. Bonner. 1983. "In Situ Vitrification of Soil." U.S. Patent 4,376,498, March 1983.

Buelt, J. L., C. C. Chapman, S. M. Barnes, R. D. Dierks. 1979. "A Review of Continuous Ceramic-Lined Melters and Associated Experience at PNL." Ceramics in Nuclear Waste Management, CONF-790420, pp. 107-113, Springfield, Virginia National Technical Information Service, April 1979. PNL-SA-7590, Pacific Northwest Laboratory, Richland, Washington.

Gray, W. J. 1980. "Volatility of Some Potential High-Level Radioactive Waste Forms," Radioactive Waste Management, Vol. 1, No. 2, pp. 147-169. Harwood Academic Publishers, New York.

Oma, K. H., D. R. Brown, J. L. Buelt, V. F. FitzPatrick, K. A. Hawley, G. B. Mellinger, B. A. Napier, D. J. Silviera, S. L. Stein, and C. L. Timmerman. 1983. In Situ Vitrification of Transuranic Wastes: Systems Evaluation and Applications Assessment. PNL-4800, Pacific Northwest Laboratory, Richland, Washington.

Oma, K. H., R. K. Farnsworth, and C. L. Timmerman. 1984. "Characterization and Treatment of Gaseous Effluents from In Situ Vitrification." Radioactive Waste Management and the Nuclear Fuel Cycle, Vol. 4, No. 4, pp. 319-341. Harwood Academic Publishers, New York, New York.

Robertson, D. E., C. W. Thomas, R. W. Perkins, and V. W. Thomas. 1981. Transuranium and Other Long-Lined Radionuclides in the Terrestrial Environs of Nuclear Power Plants. EPRI-EA-2045. Prepared by Battelle, Pacific Northwest Laboratories for Electric Power Research Institute, Palo Alto, California.

Timmerman, C. L., R. A. Brouns, J. L. Buelt, and K. H. Oma. 1983. "In Situ Vitrification: Pilot-Scale Development." Nuclear and Chemical Waste Management, Vol. 4, No. 3, pp. 267-276. Pergamon Press Inc. Elmsford, New York.

Timmerman, C. L. and R. O. Lokken. 1984. "Characterization of Vitrified Soil Produced by In Situ Vitrification." Nuclear Waste Management, Advances in Ceramics, Vol. 8, pp. 619-626. The American Ceramic Society, Columbus, Ohio.

APPENDIX A

RADIOCHEMICAL ANALYTICAL PROCEDURES
PILOT-SCALE RADIOACTIVE TEST

APPENDIX A

RADIOCHEMICAL ANALYTICAL PROCEDURES PILOT-SCALE RADIOACTIVE TEST

GAMMA-RAY SPECTROMETRY MEASUREMENT PROCEDURE

A gamma-ray spectrometer using a 100 cc intrinsic germanium detector was employed for sample analysis. The system resolution was 2 keV for the 1332.5 keV gamma-ray of ^{60}Co. The analysis system was maintained for both quality control and quality assurance using NBS traceable radionuclides of ^{241}Am (59.5 keV) and ^{60}Co (1332.5 keV). These photons allowed both gain and zero adjustments to be maintained throughout the period of measurement. To determine the appropriate efficiencies for each of the various sample types, specific mock-up assemblies containing known quantities of NBS traceable radionuclides were placed in the same position as the unknown sample being measured. Using the generated efficiency factors for each sample type, as well as the gain and zero calibration, the gamma-ray spectra were analyzed for the specific radionuclide concentrations of interest.

PROCEDURE FOR REMOVING Pu AND Sr FROM SOIL SAMPLES

1. Weigh out up to 200 g of soil into a clean beaker
   - Soil should be clean and dry.
   - Want ~2 d/m/100 g soil.
   - To insure spike absorption on soil.
2. Add slowly up to 300 ml of cold, conc. HCl
   - Sample will foam due to formation of CO_2.
3. Stir well on hot plate using large glass stirring rod.
   Heat to near boiling.
   - Do not want sample to bump but be at near boiling for 1 hour.
4. Add sufficient conc. HCl to bring volume one inch over sample.
   - Add after foaming ceases.

5. After 1 hour at near boiling, cool slightly, decant and then filter using 8.5 cm fiberglass filters.

6. Wash precipitate (ppt) with H_2O then recombine filter and ppt with original residue left in beaker.

7. Quantitatively transfer leachate to a beaker and start evaporation on hot plate.

8. Repeat steps 4 through 7 with conc. HCl; then with H_2O.
   - The water leach is to get rid of residual HCl.

9. On the H_2O leach, transfer all the residue onto the filter and let dry.

10. Combine H_2O with previous acid leachates and make to know volume; transfer ppt into a clean, labeled polybag for gamma-ray spectrographic analysis.
    - The leached soil can be dried then sealed in the polybag for storage.

PROCEDURE FOR REMOVING Pu AND Sr FROM VITRIFIED SOIL SAMPLE

1. Weigh out to 100 gram of sample and break into small pieces. Add pieces to shatter box and grind to fine powder. Transfer aliquot of fine powder to teflon beaker.

2. Add conc. HF and heat for several hours. Add conc. HNO_3 and evaporate to low volume.

3. Cool, dilute to 4 M HNO_3, filter, save both residue and supernate.

4. Place residue back in teflon beaker and repeat steps 2 and 3 twice.

5. Save residue for gamma counting. To combined HNO_3 acid supernates, make to known volume for Sr and Pu analysis.

Pu PROCEDURE

1. To aliquot, add ^{242}Pu tracer and HNO_3 to make 10 M. Add spatula tap $NaNO_2$. Heat. Allow sample to stand for 2 hours or longer.
   - Solution must be about 8 M HNO_3.
   - $NaNO_2$ reduces Pu^{+6} to Pu^{+4} and oxidizes Pu^{+3} to Pu^{+4} which is strongly absorbed on Dowex-1.

2. Pass the solution through an equilibriated Dowex-1 resin column 2.4 cm diameter by 8 cm long at the rate of 4 ml/min.
   - Do not let the column go dry.

3. Wash the column with 5 column volumes of 10 M HNO_3 and save the eluant and wash for Am and Cm procedures.
   - Do not let the column go dry.

4. Wash the column with 5 column volumes of 10 M HCl. Discard wash.
   - Removes thorium. Avoid mixing 10 M HNO_3 and 10 M HCl as much as possible to prevent gas formation.

5. Elute Pu with 5 column volumes 0.1 M ammonium iodine (NH_4I) in 10 M HCl. Allow column to go to dryness and save solution.

   Note: 0.0142 g/ml or 28 g NH_4I in 276 m of deionized H_2O diluted to 2 liters with conc. HCl = 0.1 M NH_4I.

6. To the eluant solution add 50 to 100 ml conc. HNO_3 to remove iodine.

7. Change from HCl to HNO_3 form.

   Note: A clear solution indicates HNO_3 form.

8. Increase volume to 150-200 ml with conc. HNO_3 and add $NaNO_2$ (few grains) and allow to stand 2 hours or longer.

   Note: $NaNO_2$ oxidizes Pu^{+3} to Pu^{+4}.

9. Adjust sample to 9 M HNO_3.

10. Equilibrate anion column with 5 column volumes 9 M HNO_3.

11. Pass sample solution through column and wash with 10 column volumes 9 M HNO_3.

12. Repeat steps 2, 3, and 4.

13. Elute with 5 column volumes 0.1 M NH_4I in 10 M HCl. Allow column to go to dryness and save solution.

14. Repeat steps 6 and 7.

SEPARATION OF ^{90}Sr FROM SOIL SAMPLES

1. To aliquot of leachate, dilute with H_2O, add 20 mg Sr carrier.
2. Add $Na_2C_2O_4$ powder with stirring, neutralize the acid to about a pH ~3 using NaOH.
   - A ppt will form leaving most of the Fe in solution as oxalate complex.
3. Filter through a fiberglass filter.
4. Transfer the ppt to a clean beaker with H_2O then add an excess of Na_2CO_3 powder and stir with heating for 20 minutes.
   - This will convert from the $C_2O_4^{=}$ to the $CO_3^{=}$ precipitant form.
5. Filter the ppt using fiberglass filter.
6. Dissolve the ppt in a minimum of conc. HNO_3.
7. Add fuming HNO_3 acid to ppt $Sr(NO_3)_2$. Centrifuge and save ppt.
8. Dissolve ppt with H_2O and repeat step 7 twice.
9. Dissolve ppt with H_2O, add Na_2CO_3 and centrifuge.
10. Transfer ppt to weighted planchette, dry, weigh for yield and beta count immediately for ^{90}Sr before ingrowth of ^{90}Y.

APPENDIX B

RADIONUCLIDE CONCENTRATION DATA FROM THE CORE SAMPLES

TABLE B.1. Preliminary Gamma Scan of Core Samples

Core	Depth (inches)	Core Weight	Radionuclide Concentration (pCi/g) ^{241}Am	^{137}Cs	^{106}Ru	^{60}Co	
A	0.0-9.5	334	1828	4060	11640	2260	
	9.5-16.5	622	1234	3080	514	332	
	16.5-22.0	727	1406	3640	100	258	
	22.0-27.0	588	1454	3640	161	258	
	27.0-31.0	718	564	1446	25	95	
	31.0-37.5	1126	1184	3420	28	234	
	37.5-51.0	853	1052	3040	4920	2360	
			1186	3128	1735	734	A Wt Ave
B	0.0-11.0	680	836	2160	2280	1164	
	11.0-16.0	173	2280	5280	1028	868	
	16.0-20.0	268	1930	4860	86	330	
	20.0-22.0	277	1674	4220	230	334	
	22.0-25.0	399	1446	3920	276	380	
	25.0-43.5	1148	1200	3260	814	736	
			1324	3450	971	720	B Wt Ave
C	11.0-17.0	649	536	1460	696	558	
	17.0-28.5	988	1218	3140	37	230	
	28.5-33.0	909	1058	3040	84	228	
	33.0-44.0	544	1234	2940	2400	1658	
			1031	2723	605	550	C Wt Ave
D	0-16.0	867	1352	3120	82	230	
	16.0-20.0	507	1348	3400	70	228	
	20.0-25.0	557	2680	7120	177	582	
	25.0-30.0	684	1764	4060	74	292	
	30.0-38.0	1076	1384	3700	91	302	
	38.0-51.0	909	1262	3260	1760	1108	
			1563	3938	425	472	D Wt Ave
E	0-14.0	939	1118	2960	102	232	
	14.0-17.0	531	1326	3420	470	326	
	17.0-28.0	1163	1198	3600	73	244	
	28.0-35.5	892	1202	3380	91	250	
	35.5-52.0	801	1352	3460	1024	600	
			1226	3368	308	319	E Wt Ave
F	0-11.0	522	768	1926	2220	662	
	11.0-24.0	1064	1196	3520	384	342	
	24.0-32.5	1087	1236	3640	73	258	
	32.5-35.0	350	1362	3780	52	260	
	35.0-45.5	1125	1342	3540	94	266	
	45.5-51.0	160	1310	2620	11000	4580	
			1210	3350	820	490	F Wt Ave
G	0-15.0	985	564	1606	123	173	
	18.0-23.0	788	1362	3880	45	258	
	23.0-32.5	1046	1320	3840	67	262	
	32.5-38.5	826	1282	3440	1222	740	
			1116	3154	339	345	G Wt Ave
			1246	3326	768	516	Total Wt Ave
			415	1017	2615	844	Std Dev

TABLE B.2. Selective Analysis of Crushed Core Samples

Core	Depth (inches)	Radionuclide Concentration (pCi/g) ^{241}Am	^{239}Pu	^{238}Pu	^{137}Cs	^{106}Ru	^{90}Sr	^{60}Co	
A	0-9.5	1,230	1,502	570	3,660	14,000	327,000	2,150	
	9.5-16.5	918	848	234	2,680	1,690	206,000	571	
	16.5-22.0	1,220	1,223	590	3,500	199	286,000	271	
	22.0-27.0	1,220	1,492	615	3,620	67	198,000	239	
	27.0-31.0	1,220	1,802	679	3,650	68	367,000	232	
	31.0-37.5	1,570	1,704	631	4,070	96	193,000	256	
	37.0-51.0	327	771	303	1,420	57,900	94,500	21,500	
		1,101	1,335	517	3,229	10,574	238,786	3,603	A Ave
B	0-11.0	671	857	307	1,990	1,760	142,000	651	
	11.0-16.0	854	4,209	1,030	2,520	170	141,000	271	
	16.6-20.0	1,210	1,924	694	3,570	85	202,000	225	
	20.0-27.9	879	2,914	728	2,410	499	92,400	279	
	22.0-25.0	1,460	1,882	650	3,790	120	239,000	297	
	25.0-28.0	1,230	1,551	616	3,700	68	215,000	245	
	25.0-38.0	1,460	1,357	566	3,890	76	270,000	297	
	28.0-35.0	1,310	1,419	564	3,970	71	247,000	249	
	35.0-43.5	1,390	2,038	759	3,850	205	138,000	345	
		1,163	2,017	657	3,299	339	187,378	318	B Ave
C	11.0-17.0	424	464	159	1,210	288	82,200	373	
	17.0-28.5	1,080	838	301	2,830	128	99,900	252	
	28.5-33.0	1,460	1,687	619	4,040	94	237,000	272	
	33.0-40.0	1,600	1,332	523	3,930	343	190,000	509	
		1,141	1,080	401	3,003	213	152,275	352	C Ave
D	0-7.0	1,760	1,176	405	4,570	222	99,800	411	
	7.0-13.0	1,490	1,201	418	3,640	85	168,000	226	
	13.0-16.0	1,260	697	257	3,160	69	171,000	224	
	16.0-20.0	1,320	1,026	359	3,880	70	85,600	254	
	20.0-25.0	1,620	1,116	397	4,160	75	151,000	283	
	25.0-28.0	1,720	1,113	405	4,360	130	173,000	289	
	28.0-30.0	1,900	1,402	554	3,900	139	257,000	351	
	30.0-32.0	1,710	1,292	512	4,460	268	177,000	557	
	32.0-38.0	1,390	1,228	317	3,900	75	312,000	265	
	38.0-42.0	1,730	1,329	523	4,130	148	224,000	310	
	42.0-51.0	1,340	1,848	626	3,710	247	184,000	371	
		1,567	1,221	434	3,988	139	182,036	322	D Ave
		1,289	1,459	513	3,489	2,563	192,561	1,065	A-D Ave
		375	701	186	834	10,570	73,640	3,808	Std Dev

DISTRIBUTION

No. of Copies

27 DOE Technical Information Center

R. D. Smith
Division of Waste Management
Nuclear Regulatory Commission
Washington, DC 20555

4 DOE Terminal Waste Disposal and Remedial Action
GTN
Washington, DC 20545
ATTN: J. E. Baublitz, NE-24
F. E. Coffman, NE-20
J. A. Coleman, NE-25
D. J. McGoff, NE-23

4 DOE Office of Defense Waste and Byproducts Management
GTN
Washington, DC 20545
ATTN: J. E. Dieckhoner, DP-122
J. J. Jicha, DP-123
D. B. Leclaire, DP-12
J. T. D'Ambrosia

4 Office of Geologic Repository Deployment
DOE Office of Civilian Radioactive Waste Management
RW, GTN
Washington, DC 20545
ATTN: J. W. Bennett, RW-20
C. R. Cooley, RW-24
C. H. George, RW-3
R. Stein, RW-21

R. H. Bauer
Office of Storage and Systems Development
DOE Office of Civilian Radioactive Waste Management
RW-30, Forrestal
Washington, DC 20585

No. of Copies

Dan L. Williams
Executive Director
Illinois Comm. on Atomic Energy
524 S. Second St., Rm. 415
Springfield, ILL 62706

J. O. Neff
DOE National Waste Terminal Storage Program Office
505 King Avenue
Columbus, OH 43201

3 Hazardous Chemical Waste Management Program
Oak Ridge National Laboratory
P.O. Box X
Oak Ridge, TN 37831
ATTN: D. Eyman
T. Rowe
T. Ashwood

2 Oak Ridge National Laboratory
P.O. Box X
Oak Ridge, TN 37831
ATTN: N. H. Cutshall
D. E. Large

2 U.S. Environmental Protection Agency
26 W. St. Clair Street
Cincinatti, OH 45268
ATTN: D. E. Sanning
N. B. Schomaker

Robert D. Mutch, Jr.
AWARE Inc.
80 Airport Rd.
West Milford, NJ 07480

H. T. Smith
EG&G Idaho
P.O. Box 1625
Idaho Falls, ID 83415

No. of Copies

M. H. McFadden
DOE Albuquerque Operations Office
P.O. Box 5400
Albuquerque, NM 87115

B. Rawles
Battelle Memorial Institute
Office of Nuclear Waste Isolation
505 King Avenue
Columbus, OH 43201

3 Rockwell International
Rocky Flats Plant
P.O. Box 464
LA1001 TWSO
Golden, CO 80401
ATTN: L. Smith
T. Nielson
P. Hagen

2 Technical Division
USA THAMA
Aberdeen Proving Ground, MD 21010
ATTN: W. E. Sisk
R. P. Bartell

2 Electric Power Research Institute
3412 Hillview Avenue
P.O. Box 10412
Palo Alto, CA 94304
ATTN: R. Williams
R. Komai

Jim Cornette
AFATL/DLOE
Eglin A.F.B., FL 32542

Thomas J. Walker
AFESC
Tyndall A.F.B.
Panama City, FL 32403

No. of Copies

J. L. Knabenschuh
Nuclear Fuels Services, Inc.
P.O. Box 191
West Valley, NY 14171

R. Canter
Naval Energy and Environmental Support Activity
Port Hueneme, CA 93043

2 Environmental Planning Division
Headquarters Air Force Logistics Command
Engineering and Services/DEPV
Wright-Patterson A.F.B., OH 45433
ATTN: D. R. Main
H. C. Russell

ONSITE

9 DOE Richland Operations Office

E. A. Bracken
M. Dayani
O. J. Elgert
N. T. Karagianes
J. J. Krupar, Jr.
O. L. Olson
H. E. Ransom
M. W. Shupe
J. D. White

16 Rockwell Hanford Operations

B. N. Anderson
J. L. Ash
M. A. Christie
K. A. Gasper
R. J. Gimera
R. N. Gurley
R. A. Kaldor
H. E. McGuire
D. E. McKinney
J. W. Patterson
J. H. Roecker
P. F. Salter
W. W. Schulz

No. of Copies

Rockwell Hanford Operations

D. D. Wodrich
D. E. Wood
File Copy

UNC United Nuclear Industries

T. E. Dabrowski

Westinghouse Hanford Company

A. G. Blasewitz

112 Pacific Northwest Laboratory

W. F. Bonner
R. A. Brouns
J. L. Buelt
J. G. Carter
D. B. Cearlock
T. D. Chikalla
C. R. Cole
G. W. Dawson
D. W. Dragnich
V. F. FitzPatrick (10)
R. M. Fleischman
C. A. Geffen
W. A. Glass

No. of Copies

Pacific Northwest Laboratory

J. E. Hansen
C. R. Hann
J. H. Jarrett
M. R. Kreiter
L. T. Lakey
J. M. Latkovich
R. C. Liikala
R. P. Marshall/L. D. Williams
J. L. McElroy
J. E. Mendel/M. D. Merz
J. E. Minor/D. H. Siemens
L. G. Morgan
I. C. Nelson/J. G. Stephan
R. E. Nightingale
K. H. Oma (10)
A. M. Platt
D. J. Silviera
S. L. Stein
C. W. Thomas/J. H. Reeves
C. L. Timmerman (50)
R. P. Turcotte/G. L. McVay
C. M. Unruh/E. C. Watson
B. E. Vaughan
R. E. Westerman
W. R. Wiley
Technical Information (5)
Publishing Coordination (2)